THESIS

GEOMORPHIC RESPONSES TO POST-GRAZING RECOVERY AND STREAM RESTORATION IN SEMIARID GRASSLAND STREAMS

Submitted by

Owen Richardson

Department of Geosciences

In partial fulfillment of requirements

For the Degree of Master of Science

Colorado State University

Fort Collins, Colorado

Summer 2026

Master's Committee:

Advisor: Ellen Wohl

Ryan Morrison
Joel Pederson

ABSTRACT

GEOMORPHIC RESPONSES TO POST-GRAZING RECOVERY AND STREAM RESTORATION IN SEMIARID GRASSLAND STREAMS

Semiarid grassland streams are highly sensitive to land use, climate, extreme discharges, and internal geomorphic thresholds that drive episodic erosion. Rooted in a process-based philosophy and commonly applied to historically wood-rich, beaver-modified systems, the application of low-tech process-based restoration through structures such as post-assisted log structures, beaver dam analogs, and rock-based designs is increasingly being extended to other geomorphic settings, including semiarid grasslands. In these wood-poor systems with fine-grained substrate, channel adjustment depends less on wood-mediated complexity or interactions with large clasts and more on subsurface soil piping and asynchronous responses to changing boundary conditions. Here, I evaluate post-grazing recovery and structural restoration outcomes at transect-to-landscape scales in two Southern Plains Land Trust preserves in southeastern Colorado. Following grazing cessation, soil compaction decreased after roughly a decade of rest, as indicated by a multivariate linear regression analysis of 238 soil bulk density samples. In contrast, visible above-ground upland vegetation appears to recover on timescales longer than the observation window (>10 years), based on analyses of growing-season composite Landsat imagery from 2013–2024. Logistic regression models indicate that the performance of restoration structures depends strongly on drainage area, slope, local vegetation cover, and the recency of large-scale commercial grazing. In total, only ~30% of the 92 in-channel structures evaluated (mostly ≤4 years old) were both intact and produced visible geomorphic change.

Structures in piping-dominated headwaters remained intact but rarely trapped sediment, whereas those in larger catchments were more likely to initiate local geomorphic change, despite having higher odds of destruction during peak flows. Simple numerical modeling suggests that changes in soil surface macroporosity—driven by land-use impacts on vegetation root communities, enhanced desiccation cracking, or shifts in burrowing animal populations—can influence water delivery to perched saturated layers and the initiation of soil piping. Collectively, these findings highlight the need to match restoration strategies with the geomorphic processes driving channel adjustment and call into question the extent to which commonly implemented structure-based interventions in grassland systems can be considered truly process-based.

ACKNOWLEDGEMENTS

Research is inherently collaborative, and this project is no exception. I benefited greatly from the thoughts and labor of many. First, I would like to thank my advisor, Ellen Wohl, for encouraging me to stay curious and continue asking questions. Ellen's ability to juggle not only my onslaught of questions but also to mentor and support an entire lab is truly impressive. I am eternally grateful to have been mentored and inspired by her. The fluvial family supported me in this work through friendship and hours of conversation. Katie Larkin, Lindsey Blehm, and Shayla Triantafillou provided invaluable company and help in the field.

The Colorado State University Department of Geosciences is uniquely collaborative, and I am grateful to have benefited from the mentorship and friendship of many. In particular, I am thankful to Michael Ronayne for his guidance in groundwater modeling and hydrogeology.

This research was funded by the Southern Plains Land Trust, the Colorado Riparian Association, and the Colorado Scientific Society. I would like to thank the Southern Plains Land Trust team—particularly Henry Pollock, Judith Westveer, Jay Tutchton, Kieran Andreoni, and Riley Gronemeyer—for their logistical support, field assistance, and insights into land use history.

Finally, and most importantly, I would like to thank my parents and sisters for encouraging me to stay true to myself and pursue a path of curiosity and learning. I was so excited to bring my parents to my field site, and I am glad they got to experience the joys of fluvial geomorphology with me.

TABLE OF CONTENTS

LIST OF TABLES

LIST OF FIGURES

CHAPTER 1: BACKGROUND

1. Semiarid Grassland Streams

Grasslands cover roughly 40% of Earth's terrestrial surface and support extensive river networks that respond sensitively to both natural and human disturbances (Blair et al., 2014). In southeastern Colorado, the Southern Plains Land Trust (SPLT) has been restoring grassland streams in the semiarid Mud Creek and Rule Creek catchments since 2013 as part of its broader mission to protect and restore the shortgrass prairie ecosystem. SPLT manages much of the upper Mud Creek catchment within its Heartland Ranch Preserve, which encompasses ephemeral headwater streams upstream and incised intermittent and perennial reaches downstream. Within the Rule Creek catchment, streams in SPLT's Raven's Nest Preserve are generally representative of the incised intermittent channels. Both Mud Creek and Rule Creek ultimately drain to the Arkansas River.

The diversity of hillslope and fluvial geomorphic processes across semiarid grassland streams lends itself to two distinct channel process domains (Figure 1), as exemplified by channels on the SPLT preserves. The two process domains identified within SPLT's preserves—ephemeral headwaters and incised channels—are widely observed across the Great Plains and other semiarid grasslands.

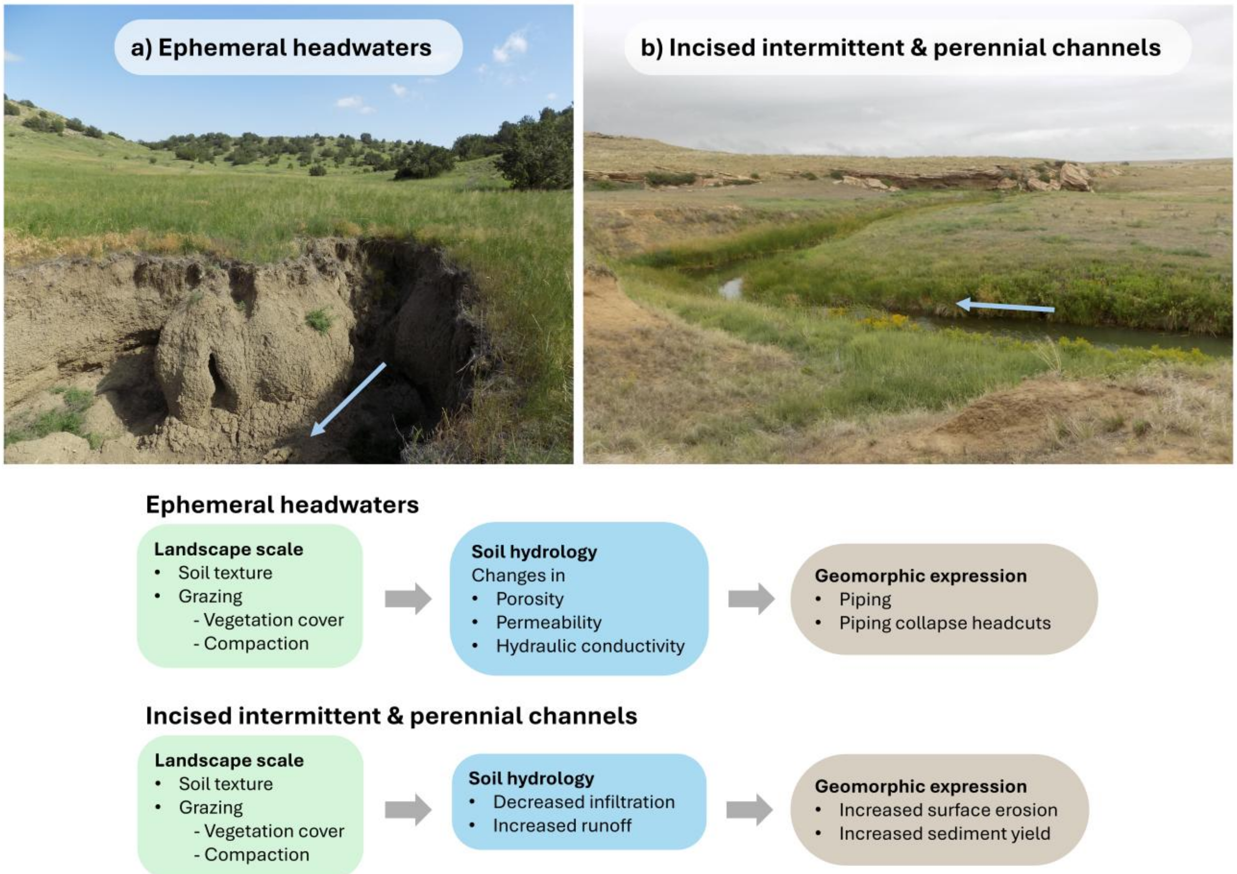

Figure 1: Key processes and drivers shaping channel morphology and landscape evolution in semiarid plains systems for (a) the ephemeral headwaters and (b) incised intermittent and perennial channels. Primary flow direction shown in blue.

A third process domain is represented by large rivers draining grassland regions, including the Arkansas, Platte, and Missouri Rivers in North America. These perennial rivers historically had a braided planform but they are now profoundly modified by large-scale channel engineering, flow regulation, extensive changes in land cover, groundwater pumping and irrigation return flows, and are not the focus of this study (Williams, 1978; Nadler & Schumm, 1981; Johnson, 1994).

1.1 Ephemeral Headwaters: Piping Collapse Networks

The first process domain consists of ephemeral headwaters, where steeper channels experience episodic surface flow. These channels often emerge from the outlets of soil piping networks, and piping collapse dominates channel initiation. Piping occurs when infiltrating water concentrates into subsurface macropores, and erosion around these pores enlarges them into subsurface “pipes” (Barendregt & Ongley, 1977; Bryan & Jones, 1997). When piping conduits collapse, they form amphitheater-shaped subsidence features at the surface (Figure 1a). Piping is a known driver of subsurface erosion throughout all major hydroclimatic regions; studies of gully initiation spanning sites in Colorado, California’s Sacramento Valley, Missouri, England, Nigeria, Israel, Spain, Tunisia, Lesotho, Canada, Australia, New Zealand, and South Africa have shown that piping is often a significant, even dominant, contributor to gully development (Dardis & Beckedahl, 1988; Higgins, 1990; Bocco, 1991; Bryan & Jones, 1997). Swanson et al. (1989) demonstrated that piping can sometimes carry far greater discharges than surface flow and has been responsible for extensive gullying in some coastal California catchments. Clearly, piping is an important and often underrecognized driver of gully erosion.

The specific processes that contribute to the development of macroporosity are highly variable across different hydroclimatic and geomorphic settings (Bryan & Jones, 1997). In semiarid areas, piping tends to occur when a permeable layer lies above local base level, providing a medium in which macropores can develop (Barendregt & Ongley, 1977). Shrink-swell clays such as montmorillonite commonly produce desiccation cracks that enhance infiltration into susceptible layers. Dispersible clays in such layers are easily mobilized during high-intensity rainfall events, initiating pipe erosion. Pipe outlets often begin as seepage faces, subsequently enlarging into distinct conduits that eventually collapse (Barendregt & Ongley, 1977; Bryan & Jones, 1997). Pipe formation is enhanced along contacts with variable hydraulic conductivity, particularly over impervious layers in or below the C horizon and in areas with steep hydraulic gradients (Schumm, 1966; García-Ruiz et al., 1997). In semiarid regions, soil pipes are large (~1 m diameter, compared to 20-40 cm in other environments) and subsidence following the erosion of pipes is of significant concern to farmers and ranchers (Bryan and Jones, 1997). Anthropogenic land use, through its impacts on vegetation cover and soil compaction, may alter infiltration and piping processes (Floyd, 1974).

At SPLT, field evidence such as amphitheater-shaped headcuts with no upstream signs of surface flow suggests that piping processes have heavily influenced channel morphology in the headwaters of Mud Creek and Rule Creek (Figure 1a). The collapse of piping networks may limit the ability of surface erosion control structures to address headcut erosion in the ephemeral headwaters process domain, since piping is a subsurface process.

1.2 Intermittent and Perennial Channels: Arroyo Incision

The second process domain consists of intermittent to perennial arroyo channels, which may have originated through piping, surface erosion, or some combination of the two, but are now shaped by surface flows that both erode and deposit sediment. Arroyos are defined here as incised semiarid channels with steep banks that disconnect flow from adjacent alluvial surfaces, including former floodplains that now serve as terraces. Many channels within the Mud and Rule Creek catchments can be described as arroyos. The causes of arroyo incision in semiarid landscapes have been highly debated within geomorphology since at least the 1880s, and numerous studies have since been published. This body of work suggests many possible explanations for rapid arroyo incision (summarized in

Table 1), generally focused on the “cows versus climate” debate (Aby, 2017).

Early works on arroyo incision investigated decadal scale incision and aggradation in the arid to semiarid American Southwest, often acknowledging grazing as a contributing factor to downcutting (Bryan, 1928; Burkham, 1966). Trimble and Mendel (1995) discussed post-grazing geomorphic recovery, emphasizing that cattle have particularly detrimental impacts on riparian vegetation and bank stability. Areas with heavy grazing are more likely to experience decreased infiltration and subsequent geomorphic impacts than moderate or light grazing. They also noted that vegetation cover may control a threshold response such that areas with low vegetation cover (<40%) are especially vulnerable to increases in surface erosion due to grazing (Graf, 1979; Zöbisch, 1993; Trimble & Mendel, 1995). Similarly, Gellis et al. (1991) observed that vegetation colonization in entrenched arroyo channels can lead to decreased sediment loads and improved channel stability. Lane (2017), in an analysis of natural flood management, noted that cattle grazing can cause soil compaction and reduced infiltration capacity, leading to greater surface runoff, flashier flood peaks, and associated geomorphic impacts. Together, grazing-driven soil compaction and vegetation loss provide clear mechanisms linking land use to arroyo development.

As research into arroyo development progressed, geomorphologists also began to examine climatic shifts as possible explanations for decadal- to century-scale cycles of alternating incision and aggradation in dryland channels. Wet periods could generate larger, more erosive flows, whereas dry periods could lead to vegetation die-offs that destabilize soils and reduce resistance to erosion (Huntington, 1914; Gregory, 1915; Leopold, 1951). Some suggested that both outcomes were simultaneously possible: periods of moderate precipitation corresponded to low rates of geomorphic change, while crossing a threshold in either the wet or dry direction could trigger change (Richardson, 1945; Langbein & Schumm, 1958). Others have pointed to extreme precipitation and extreme discharge events, and their interactions with the river corridor, as distinct drivers of geomorphic change in dryland streams (Dellenbaugh, 1912; Hereford, 2002; Perignon et al., 2013).

Patton and Schumm (1975) described arroyo incision as a geomorphic threshold phenomenon—an intrinsic property of fluvial systems, rather than a response to external forcing—based on an observed relationship between the drainage area and valley slope of incising versus stable alluvial channels. At a given drainage area, channels that exceed a critical slope are more prone to arroyo formation. More broadly, studies by Schumm and Hadley (1957), Schumm and Parker (1973), Schumm (1975), and Gellis et al., (1991) argued that arroyo incision is an inherent and recurring process in semiarid drainages, with episodic trenching occurring throughout the Quaternary as an asynchronous, complex response to base level changes and the crossing of geomorphic thresholds. Recent chronostratigraphic studies indicate that arroyo incision depends on both sediment supply and hydroclimatic transitions; increased flood magnitude and frequency can initiate incision once systems have aggraded toward a geomorphic threshold in response to prolonged drought or land-use change (Harvey & Pederson, 2011; Townsend et al., 2019). In this framework, climatic variability initiates incision, with antecedent fine sediment aggradation rendering channels sensitive to base-level change. Periods of prolonged drought or land use may supply this fine sediment to the channel, after which further adjustment proceeds through autogenic, catchment-specific processes, producing spatially variable and asynchronous incision and aggradation (Gellis et al., 1991; Phippen & Wohl, 2003; Tucker et al., 2006; Harvey & Pederson, 2011; Townsend et al., 2019).

Table 1. Mechanisms for rapid arroyo incision and selected examples.

Mechanism	Explanation	Examples
Land use	Land use changes following European colonization—particularly cattle grazing and unpaved road development—compact soils, reduce infiltration and concentrate runoff, increasing flow erosivity and sediment yield.	Bryan, 1928; Burkham, 1966; Phippen & Wohl, 2003
Wetter climate	A wetter climate increases discharge, stream power, and the capacity for flows to erode the bed and banks.	Gregory, 1915; Richardson, 1945; Langbein & Schumm, 1958; Townsend et al., 2019
Drier climate	A drier climate reduces vegetative cover and destabilizes soils, decreasing resistance to erosion and enhancing upstream knickpoint propagation.	Huntington, 1914; Richardson, 1945; Leopold, 1951; Langbein & Schumm, 1958
Extreme events	Extreme precipitation and subsequent extreme discharge events drive increased flow erosivity and arroyo incision.	Dellenbaugh, 1912; Hereford, 2002; Harvey & Pederson, 2011; Perignon et al., 2013; Townsend et al., 2019
Intrinsic properties	Slope-drainage area relations, width-depth ratios, and other fluvial thresholds can reactivate drainage networks, with complex response producing spatiotemporally discontinuous cycles of incision and aggradation in response to a single base level change.	Schumm & Hadley, 1957; Schumm & Parker, 1973; Patton & Schumm, 1975; Schumm, 1975; Gellis et al., 1991; Harvey & Pederson, 2011; Townsend et al., 2019

Table 1 summarizes commonly proposed mechanisms of arroyo incision and aggradation and provides a non-exhaustive selection of representative examples from the literature. At a fundamental level, periodic arroyo incision should be understood as a natural component of semiarid geomorphic systems that occurred in the Western United States prior to European settlement and associated changes in land cover, rather than as a strictly detrimental or anthropogenic disturbance. However, it is important to recognize the additional geomorphic impacts caused by cattle grazing, and to consider the potential for landscape response following cattle removal at SPLT.

2. Study Area

Heartland Ranch Preserve (174 km^2) and Raven's Nest Preserve (19 km^2), located in Bent County in southeastern Colorado, are the largest preserves managed by the Southern Plains Land Trust (Figure 2). SPLT began acquiring land at Heartland and Raven's Nest through direct purchase in 2013 and has since continued expanding the preserves parcel by parcel. As a result, Heartland has a piecemeal land-use history, with many distinct grazing histories reflecting different stages of cattle removal during the acquisition by SPLT.

For the purposes of this study, grazing is divided into two categories based on the last presence of large-scale commercial beef cattle grazing operations: historic and recent. Under commercial grazing, the peak annual cattle stocking rate was estimated from an approximate herd size of two thousand cows per growing season per area, yielding a value of roughly 0.115 AUM ha^{-1}, where one AUM (animal unit month) equals the monthly forage demand by a ruminant weighing 1,000 pounds, with or without a calf up to 6 months in age. Land in the "historic" grazing category had cattle removed during or prior to 2015. A second wave of land acquisition and subsequent cattle removal began in 2021; areas designated as having "recent" grazing had commercial operations through at least 2021, with some commercial grazing continuing through 2025.

After the cessation of commercial operations, SPLT reduced the stocking rate to roughly one-tenth of pre-acquisition levels, maintaining about two hundred animals on Heartland Ranch Preserve—most of them bison, along with some sterilized horses and cattle. While the specific effects of bison versus cattle are not considered in this research, bison are recognized as keystone species that influence many ecosystem processes (Knapp et al., 1999). Following formal cattle removal, bison herd management by SPLT and occasional trespass grazing have temporarily increased the stocking rate in parts of the preserves, but these are not considered a reactivation of the former commercial grazing regime. The study area and grazing regimes are shown in Figure 2.

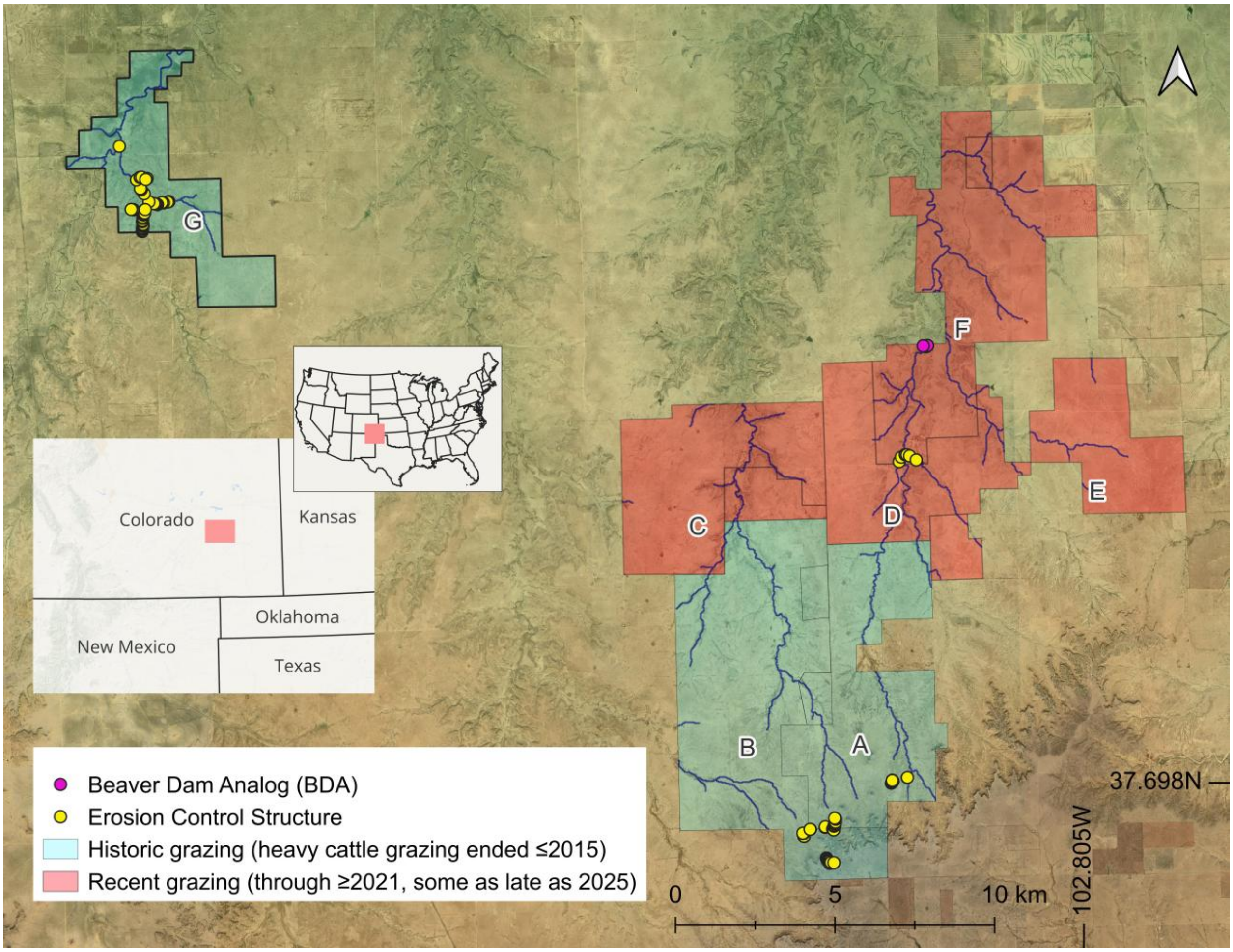

Figure 2: Study area map of the Southern Plains Land Trust near Lamar, Colorado. Parcel fill colors indicate grazing history, and in-channel restoration structures are shown as dots. Parcels are labeled as A-G.

The study area lies within a semiarid grassland characterized by flashy hydrology driven by frontal systems, convective storms, and the North American Monsoon. Annual precipitation at the nearby "Lamar 3" CoAgMET weather station (Schumacher et al., 2018) averages 34 cm/year over 2014-2024. 75% of annual precipitation falls during the growing season months of May-September.

The southern portion of Heartland Ranch features a ~40-meter-tall retreating escarpment capped by resistant limestone of the Cretaceous Niobrara Formation. The elevation of the escarpment is approximately 1440 meters above mean sea level. North of the escarpment, the terrain is flat (gently sloping northward at a gradient of ~0.005) and of low relief. From the mesa scarp region, streams flow generally northward across a dense drainage network underlain by clastic and carbonate sedimentary units of the Cretaceous Colorado Group, Dakota Formation, and Purgatorie Formation (Scott, 1968). These streams are predominantly alluvial but occasionally interact directly with bedrock. A geologic map of the study area is shown in Figure 3. Vegetation cover is dominated by perennial grasses such as buffalograss (*Bouteloua dactyloides*) and blue grama (*Bouteloua gracilis*), along with scattered shrubs and succulent plants, including yucca (*Yucca* spp.) and cholla cactus (*Cylindropuntia* spp.), characteristic of semiarid prairie systems.

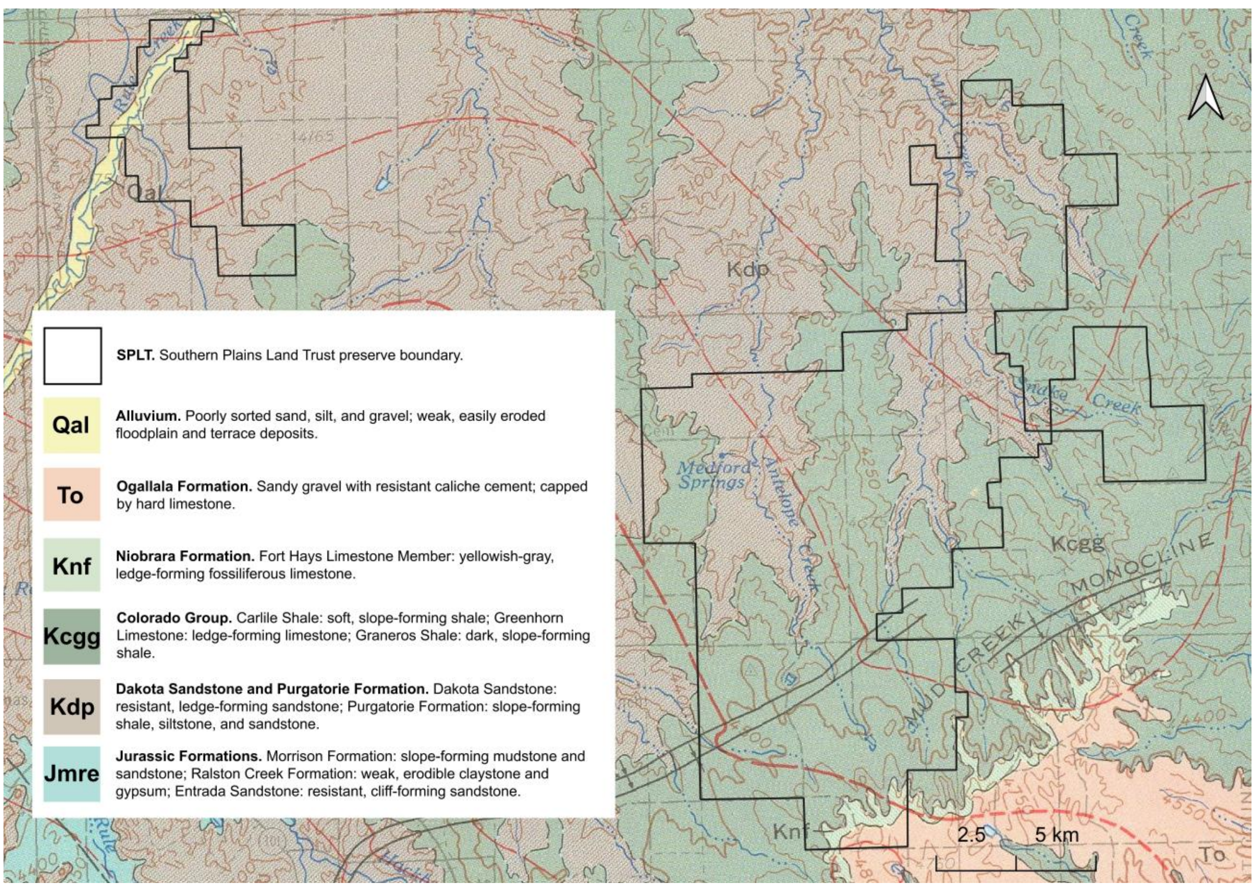

Figure 3: Generalized geologic map of the study area, from Scott (1968).

Mud Creek and Rule Creek are the primary drainage networks within Heartland Ranch and Raven's Nest, respectively. Their mainstem channels generally fall within the intermittent to perennial incised arroyo process domain, while smaller tributaries typically represent the ephemeral headwaters process domain.

References

Aby, S. B. (2017). Date of arroyo cutting in the American Southwest and the influence of human activities. *Anthropocene*, *18*, 76-88.

Barendregt, R. W., & Ongley, E. D. (1977, July). Piping in the Milk River Canyon, southeastern Alberta-a contemporary dryland geomorphic process. In *Matter Transport in Inland Waters Symposium, IAHSAISH Publication* (Vol. 122, pp. 233-243).

Blair, J., Nippert, J., & Briggs, J. (2014). Grassland ecology. In R. Monson (Ed.), *Ecology and the Environment* (pp. 389–423). Springer.

Bocco, G. (1991). Gully erosion: processes and models. *Progress in Physical Geography*, *15*(4), 392-406.

Bryan, K. (1928). Historic evidence on changes in the channel of Rio Puerco, a tributary of the Rio Grande in New Mexico. *The Journal of Geology*, *36*(3), 265-282.

Bryan, R. B & Jones, J. A. (1997). The significance of soil piping processes: inventory and prospect. *Geomorphology*, *20*, 209-218.

Burkham, D. E. (1966). *Hydrology of Cornfield Wash area and effects of land-treatment practices, Sandoval County, New Mexico, 1951-60* (No. 1831). US Government Printing Office.

Dardis, G. F. (1988). Drainage evolution in an ephemeral soil pipe–gully system, Transkei, southern Africa. In B. P. Moon (Ed.), *Geomorphological studies in southern Africa* (pp. 267–276). Balkema.

Dellenbaugh, F. S. (1912). Cross cutting and retrograding of streambeds. *Science*, *35*(904), 656-658.

Floyd, E. J. (1974). Tunnel erosion: A field study in the Riverina, New South Wales. *Journal of the Soil Conservation Service of New South Wales, 30*(3), 145–156.

García-Ruiz, J., Lasanta, T., & Alberto, F. (1997). Soil erosion by piping in irrigated fields. *Geomorphology*, *20*(3-4), 269-278.

Gellis, A., Hereford, R., Schumm, S. A., & Hayes, B. R. (1991). Channel evolution and hydrologic variations in the Colorado River basin: factors influencing sediment and salt loads. *Journal of Hydrology*, *124*(3-4), 317-344.

Graf, W. L. (1979). The development of montane arroyos and gullies. *Earth Surface Processes*, *4*(1), 1-14.

Gregory, H. E. (1915). The formation and distribution of fluviatile and marine gravels. *American Journal of Science*, *4*(233), 487-508.

Harvey, J. E., & Pederson, J. L. (2011). Reconciling arroyo cycle and paleoflood approaches to late Holocene alluvial records in dryland streams. *Quaternary Science Reviews*, *30*(7-8), 855-866.

Hereford, R. (2002). Valley-fill alluviation during the Little Ice Age (ca. AD 1400–1880), Paria River basin and southern Colorado Plateau, United States. *Geological Society of America Bulletin*, *114*(12), 1550-1563.

Higgins, C. G. (1990). Gully development. In C. G. Higgins & D. R. Coates (Eds.), *Groundwater Geomorphology: The role of subsurface water in Earth-surface processes and landforms* (Geological Society of America Special Paper 252, pp. 139–156). Geological Society of America.

Huntington, E. (1914). *The climatic factor as illustrated in arid America* (No. 192). Carnegie institution of Washington.

Johnson, W. C. (1994). Woodland expansions in the Platte River, Nebraska: patterns and causes. *Ecological Monographs*, *64*(1), 45-84.

Knapp, A. K., Blair, J. M., Briggs, J. M., Collins, S. L., Hartnett, D. C., Johnson, L. C., & Towne, E. G. (1999). The keystone role of bison in North American tallgrass prairie: Bison increase habitat heterogeneity and alter a broad array of plant, community, and ecosystem processes. *BioScience*, *49*(1), 39–50.

Lane, S. N. (2017). Natural flood management. *WIREs Water, 4*(1), e1211. https://doi.org/10.1002/wat2.1211

Langbein, W. B., & Schumm, S. A. (1958). Yield of sediment in relation to mean annual precipitation. *Eos, Transactions American Geophysical Union*, *39*(6), 1076-1084.

Leopold, L. B. (1951). Rainfall frequency: an aspect of climatic variation. *Eos, Transactions American Geophysical Union*, *32*(3), 347-357.

Nadler, C. T., & Schumm, S. A. (1981). Metamorphosis of South Platte and Arkansas rivers, eastern Colorado. *Physical Geography*, *2*(2), 95-115.

Patton, P. C., & Schumm, S. A. (1975). Gully erosion, Northwestern Colorado: a threshold phenomenon. *Geology*, *3*(2), 88-90.

Perignon, M. C., Tucker, G. E., Griffin, E. R., & Friedman, J. M. (2013). Effects of riparian vegetation on topographic change during a large flood event, Rio Puerco, New Mexico, USA. *Journal of Geophysical Research: Earth Surface*, *118*(3), 1193-1209.

Phippen, S. J., & Wohl, E. (2003). An assessment of land use and other factors affecting sediment loads in the Rio Puerco watershed, New Mexico. *Geomorphology*, *52*(3-4), 269-287.

Richardson, H. L. (1945). Discussion: the significance of terraces due to climatic oscillation. *Geological Magazine*, *82*(1), 16-18.

Schumacher, R. S., Goble, P. E., Schwalbe, Z., & Bolinger, R. A. (2018). Using CoAgMET, "Colorado's Mesonet," to analyze our state's weather and climate. *Colorado Water, 35*(5).

Schumm, S. A. (1966). The development and evolution of hillslopes. *Journal of Geological Education*, *14*(3), 98-104.

Schumm, S. A. (1975). Episodic erosion: A modification of the geomorphic cycle. In W. N. Melhorn & R. C. Flemal (Eds.), *Theories of Landform Development* (pp. 69–85). Publications in Geomorphology, State University of New York, Binghamton.

Schumm, S. A., & Hadley, R. F. (1957). Arroyos and the semiarid cycle of erosion. *American Journal of Science*, *255*(3), 161-174.

Schumm, S. A., & Parker, R. S. (1973). Implications of complex response of drainage systems for Quaternary alluvial stratigraphy. *Nature Physical Science*, *243*(128), 99-100.

Scott, G. R. (1968). *Geologic and structure contour map of the La Junta quadrangle, Colorado and Kansas* (Miscellaneous Geologic Investigations Map I-560) [Map]. U.S. Geological Survey.

Swanson, M. L., Kondolf, G. M., & Boison, P. J. (1989). An example of rapid gully initiation and extension by subsurface erosion: coastal San Mateo County, California. *Geomorphology*, *2*(4), 393-403.

Townsend, K. F., Nelson, M. S., Rittenour, T. M., & Pederson, J. L. (2019). Anatomy and evolution of a dynamic arroyo system, Kanab Creek, southern Utah, USA. *Geological Society of America Bulletin*, *131*(11-12), 2094-2109.

Tucker, G. E., Arnold, L., Bras, R. L., Flores, H., Istanbulluoglu, E., & Solyom, P. (2006). Headwater channel dynamics in semiarid rangelands, Colorado high plains, USA. *Geological Society of America Bulletin*, *118*(7-8), 959–974.

Trimble, S. W., & Mendel, A. C. (1995). The cow as a geomorphic agent—a critical review. *Geomorphology*, *13*(1-4), 233–253.

Williams, G. P. (1978). *The case of the shrinking channels—The North Platte and Platte Rivers in Nebraska* (U.S. Geological Survey Circular 781).

Zöbisch, M. A. (1993). Erosion susceptibility and soil loss on grazing lands in some semiarid and subhumid locations of eastern Kenya. *Journal of Soil and Water Conservation*, *48*(5), 445-448.

CHAPTER 2: MULTISCALE MONITORING OF POST-GRAZING RECOVERY AND RESTORATION OUTCOMES IN SEMIARID GRASSLAND CHANNELS

1. Introduction

1.1 Restoration of semiarid grassland streams

Stream restoration is a multi-billion-dollar global industry (Bernhardt et al., 2005; Bergstrom & Loomis, 2017), yet only a small fraction (~10%) of projects have historically received any post-installation assessment or monitoring. Beechie et al. (2010) advocated for process-based restoration, which focuses on restoring underlying geomorphic processes rather than simply constructing desired channel forms. A key tenet of process-based restoration is that project goals are clearly stated. Another is that the scale of restoration matches the scale of the problem, for example, interventions ranging from cattle removal at the landscape scale to in-channel structures at the reach scale. Although process-based approaches have gained prominence, many restoration projects still fail to fully meet these principles. Most stream restoration projects lack long-term monitoring, particularly those in semiarid grassland streams, which have received little formal research focus. In their management and conservation of grassland streams, SPLT aims to implement process-based restoration, and monitoring geomorphic processes is central to assessing their success.

More recently, low-tech process-based restoration (LTPBR) has gained popularity among practitioners (Scamardo et al., 2025). LTPBR builds on the principles of process-based restoration but emphasizes that structures should have a low unit cost and use locally sourced materials. Natural Infrastructure in Dryland Streams (NIDS) represent a formalized application of LTPBR principles developed specifically for arid and semiarid river corridors and wetlands. The NIDS framework describes how beaver-engineered and anthropogenic structures built from sediment, rock, wood, and other organic material are central to dryland stream functionality (Norman et al., 2022). Such structures can enhance soil, water, and carbon storage, improve hyporheic connectivity, and restore the absorptive capacity of dryland streams to respond to disturbances like floods, land use change and climate change.

SPLT has installed over a hundred individual structures broadly categorized under LTPBR and NIDS since 2013 to prevent surface erosion, enhance surface and subsurface water storage, create habitat, and meet other goals. For the purposes of this study, these structures are broadly classified as erosion control structures that attempt to create areas of elevated channel roughness and reduced flow velocity in backwater areas, thus attenuating fluxes of sediment, water, wood, and other organic matter. Many are Zeedyk structures, a specific set of hand-built, anthropogenic NIDS restoration features installed following Zeedyk and Jansens' guidelines (2009). Zeedyk structures are commonly small rock structures oriented perpendicular to flow (Figure 3), though some designs incorporate wood, straw, and fabric. Numerous studies summarized by Scamardo et al. (2025) have evaluated geomorphic, hydrologic, and ecological outcomes of LTPBR, but long-term (3+ year) assessments remain rare, especially in shortgrass prairie systems.

Beavers have increasingly been recognized as powerful agents of geomorphology. Beaver modifications enhance lateral floodplain connectivity by creating low-velocity backwater conditions that allow fine sediment to settle and deposit. They raise water levels, promote infiltration into channel banks and floodplains, and increase water storage, in the process creating aquatic and riparian habitat (Larsen et al., 2021). In parallel, Beaver Dam Analogs (BDAs) have been installed by practitioners like SPLT to mimic these effects as part of the

LTPBR movement. SPLT has thus far installed four BDAs. Beaver restoration has been shown to promote the recovery of incised channels in other geomorphic settings (Pollock et al., 2014).

Prior to the rise of low-tech process-based restoration (LTPBR) in the 2010s, several studies investigated the responses of semiarid channels to hard-engineered erosion control interventions. In Australia's Riverina agricultural region, Floyd (1974) performed physical experiments on agricultural land, finding that the mechanical destruction of piping networks through "ripping" was only temporarily effective at preventing further subsurface erosion. Landscape-scale treatments were more effective: proper grazing management that allowed for dense vegetation cover helped retain water and prevented the desiccation cracks that rapidly feed macropores and piping networks (Floyd, 1974). Likewise, ripping, sediment retention basins, and other erosion control techniques in the semiarid Western United States have been largely ineffective, either because pre-existing geomorphic conditions were disregarded or because of inadequate maintenance (Dortignac & Hickey, 1963; Phippen & Wohl, 2003). A study of a semiarid catchment in Wyoming reached similar conclusions, noting that "engineering structures to control sediment export had been constructed in poorly chosen locations at extreme and unnecessary expense to taxpayers" (Marston & Dolan, 1999). In arid and semiarid catchments, slope, vegetation cover, and soil texture are found to be predictive of soil erosion outcomes (Meeuwig, 1970; Blackburn & Skau, 1974; Marston & Dolan, 1999). Although not intended as a comprehensive planning guide, a Natural Resources Conservation Service (NRCS)-approved publication recommends low-tech surface erosion control structures for headcuts that are formed through subsurface-driven erosion. This approach risks mismatching treatment to underlying processes and could be problematic if applied broadly (Maestas et al., 2018). As emphasized by

Wohl et al. (2024), the local geomorphic context and processes operating on a river system fundamentally control restoration outcomes.

Building on this perspective, Gellis et al. (1995, 2001) analyzed erosion control structures in a semiarid catchment characterized by arroyo incision and developed a prioritization framework for restoration within the Zuni Indian Reservation in New Mexico. They highlighted the need for multiscale monitoring to improve understanding of arroyo restoration (Gellis et al., 1995), yet few studies have captured impacts beyond the reach scale. More recently, the availability of high-resolution (1 m) DEMs and advances in remote sensing now enable more comprehensive assessments of catchment-scale upland restoration.

1.2 Objectives and Hypotheses

The primary objective of this chapter is to monitor stream recovery and restoration in the ephemeral headwaters and intermittent/ephemeral arroyo process domains across multiple spatial scales, and to assess restoration and erosion control outcomes in the current restoration zeitgeist. Since SPLT owns much of the uplands within the Mud Creek catchment, I can assess not just local channel adjustments but also broader landscape evolution following cattle removal and stream restoration activity. Specifically, this work seeks to: (1) monitor, at the landscape scale, processes sensitive to land-use change, namely soil bareness and compaction; (2) evaluate how variations in these landscape characteristics, along with basin- and site-scale hydraulic conditions, influence the intactness and geomorphic effects of in-channel restoration structures; and (3) develop a flowchart-style decision framework for the Southern Plains Land Trust (SPLT) to guide future placement of in-channel structures.

Hypothesis 1a: Land use history will be a strong predictor of soil compaction.

I hypothesize that grazing history will be a strong predictor of soil bulk density, when controlling for soil texture. Livestock grazing can impact soil structure and vegetation cover through trampling and consumption, leading to increased soil compaction and reduced water infiltration (Trimble & Mendel, 1995).

Hypothesis 1b: Land use history will be a strong predictor of vegetation cover.

Likewise, I hypothesize that grazing history will be a strong predictor of vegetation cover, when controlling for growing season precipitation. Heavily grazed parcels are expected to exhibit greater bare soil exposure. Although local variation in soil texture, slope and natural disturbance history influence ground cover, differences in land use history (e.g., grazing intensity and duration) are likely to explain significant variation in vegetation conditions across the catchment.

Hypothesis 2a: In ephemeral headwaters, the success of structures installed to address gullying may be limited in areas dominated by subsurface-driven erosion, while steeper, unvegetated reaches are expected to respond more effectively to in-channel erosion control interventions.

In semiarid environments, valleys that exceed a threshold steepness (Patton and Schumm, 1975) are more prone to gully erosion. Roughness- and drag-enhancing structures, like one-rock dams (ORDs), Zuni bowls, and post-assisted log structures (PALS), can help increase frictional resistance, reduce flow velocities (and thus shear stress), and promote sediment deposition. However, because piping collapse is a dominant driver of headcut formation in the study area, I hypothesize that many structures will be ineffective at stabilizing channels where subsurface processes prevail. Steep, unvegetated reaches are more strongly influenced by surface flow processes that might be altered by structures that at least partially obstruct flow

Hypothesis 2b: In deeply incised intermittent and perennial channels, the success of beaver dam analogs (BDAs) installed to increase channel heterogeneity and lateral connectivity will depend on morphological complexity and bank conditions.

I hypothesize that BDAs are more likely to retain fine sediment and increase channel heterogeneity in areas with increased morphological complexity (such as inset floodplain presence) and shallower, non-cohesive banks. Restoration efforts aimed at creating backwater conditions and reconnecting flow to the floodplain are unlikely to succeed in reaches where floodplain access is limited or absent. Deeply incised channels with steep, cohesive banks may not respond as desired to in-channel interventions.

2. Methodology

2.1 Landscape-scale analysis

2.1.1 Soil compaction

To test Hypothesis 1a, I collected soil samples to assess bulk density. Bulk density (ρ_b) is defined as the dry weight of soil divided by its total volume, including pore spaces (McKenzie et al., 2002). To collect samples for bulk density analyses, I drove a 7.5-centimeter-diameter rigid metal cylinder with a sharpened edge into the soil surface and extracted the sample, trimming any roots or material extending beyond the cylinder before placing the material into a sample bag (McKenzie et al., 2002). The dataset is internally consistent, as all measurements were collected using the same method by a single person over the course of five days to minimize variation in collection technique. Samples were collected from surface horizons, which often contained organic material and desiccation cracks. Surface horizon bulk density has been reported as low as 0.5 Mg/m^3, lower than the typical 1.1–1.8 Mg/m^3 reported for soil profiles more generally (McKenzie et al., 2002). The known cylinder volume represents the total soil volume. I dried and weighed the bagged samples to determine bulk density.

I sampled within each distinct land-use history of Heartland Ranch Preserve and, within those parcels, across distinct soil types. More than 30 soil series are mapped within Heartland according to the NRCS Web Soil Survey (Soil Survey Staff, NRCS, 2025), with many series occurring across multiple areas of the preserve. I grouped soils into four categories based on percent sand: 0-20%, 20-40%, 40-60% and 60-80%. Lower percent sand indicates greater silt and clay content. Soils with >80% sand occurred only in one parcel and were therefore excluded, as comparison across grazing histories was not possible. I sampled ten locations within each soil-texture category and each parcel A-F (see Figure 2), resulting in 238 bulk-density samples (two samples were lost during processing). Because SPLT does not manage as much of the upper catchment at Raven's Nest, the ability to perform catchment-scale monitoring there was more limited than at Heartland. Accordingly, catchment-scale recovery analysis focused primarily on Heartland Ranch, with structure monitoring at Raven's Nest serving to supplement the evaluation of in-channel responses.

Apart from coverage of each parcel and texture class, sampling locations were otherwise determined in the field by walking thirty paces and dropping the cylinder to identify the next location. I selected starting locations to ensure coverage across the preserve while accounting for the logistical challenges of access and sample transport in SPLT's remote terrain; most sites were located within 1 km of roads. I recognize that this could introduce some systematic bias towards elevated compaction, since cattle infrastructure (e.g., water tanks, salt sources, and fence lines) influences cattle behavior and is also often located near roads for logistical purposes (Ganskopp, 2001). The historic distribution of such infrastructure could have increased local grazing intensity relative to the preserve-wide average of approximately 0.115 AUM ha^{-1}. Much of this infrastructure has since been removed, but its former presence may influence contemporary bulk density patterns.

To assess whether grazing history was associated with differences in bulk density across soil textures, I fit a multiple linear regression model with bulk density as the response variable and grazing history, texture class and their interaction as predictors (1). This model tested whether the relationship between bulk density and soil texture varied by grazing history. I then used the *emmeans* package in R (Lenth, 2025) to compute estimated marginal means and tested pairwise contrasts between parcels with historic and recent commercial grazing within each texture class, evaluating whether bulk density differed significantly between grazing histories for each texture category. All statistical analyses in this study were completed using the R programming language, with significance assessed at the 0.05 level (R Core Team, 2025).

$$\text{Bulk density} \sim \text{Texture} \times \text{Grazing} \tag{1}$$

2.1.2 Vegetation cover

To test Hypothesis 1b, I analyzed ground cover across SPLT's Heartland Ranch Preserve using Landsat 8/9 surface reflectance imagery, available beginning in 2013, prior to the establishment of the preserve. For each year from 2013 to 2024, I generated a median composite growing-season (May–September) image in Google Earth Engine and calculated the Bare Soil Index (BSI) to map spatial patterns of bare ground across the preserve (Rikimaru et al., 2002; Gorelick et al., 2017).

$$BSI = \frac{(SWIR1 + Red) - (NIR + Blue)}{(SWIR1 + Red) + (NIR + Blue)} \tag{2}$$

BSI (2) is a good fit for this study because, in vegetated areas (including areas with dead vegetation), near-infrared (NIR) reflectance is significantly higher than shortwave infrared (SWIR1) reflectance, resulting in lower BSI values. In contrast, in bare or sparsely vegetated areas, NIR and SWIR1 are more similar, or SWIR1 may slightly exceed NIR, resulting in higher BSI values (Rikimaru et al., 2002; Lillesand et al., 2015). Additionally, because both NIR and SWIR1 are similarly influenced by background soil moisture, BSI provides a relatively robust measure of surface characteristics across varying moisture conditions. BSI also accounts for differences in the visible bands, recognizing that the red-blue difference tends to be greater for barer pixels. High BSI values are therefore used as an indicator of greater surface bareness across the study area. Other indices, including the normalized difference vegetation index (NDVI) and the normalized difference moisture index (NDMI), were considered but ultimately rejected.

NDVI describes a broad array of vegetation reflectance properties rather than focusing on reflectance properties pertinent to ground cover (Huang et al., 2021). NDMI is computed in a similar fashion to BSI by differencing SWIR1 and NIR but excludes visible wavelengths. Sample spectral reflectance profiles for relatively vegetated and bare pixels from the study area are shown in Figure 4.

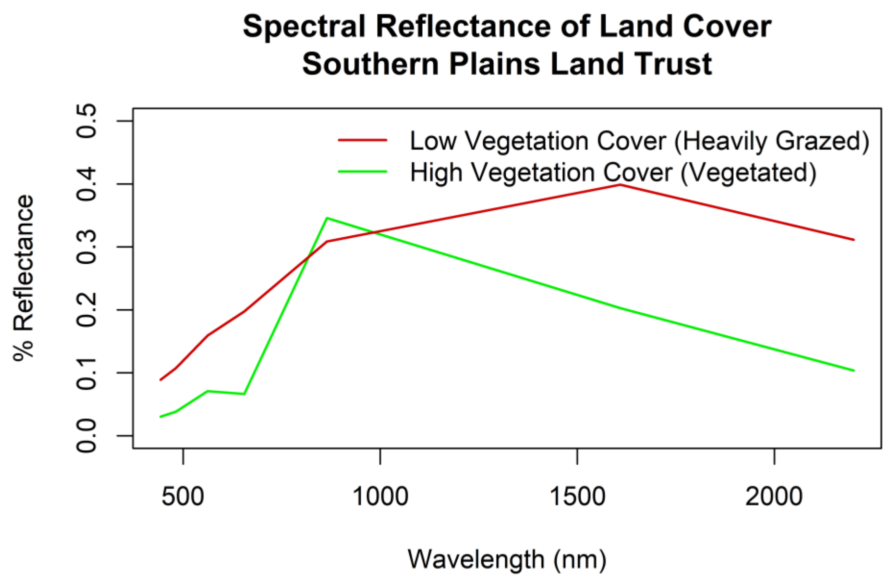

Figure 4: Sample spectral reflectance profiles for relatively vegetated and bare pixels from SPLT's Heartland Ranch Preserve.

I extracted the median BSI for each parcel and year using the *terra* package in R (Hijmans, 2025) and fit a multiple linear regression model with median BSI as the response variable and growing-season precipitation, year, grazing history, and the year-grazing interaction as predictors (3). Growing-season precipitation was calculated as the sum of precipitation over May 1st to September 30th from the "Lamar 3" CoAgMET rain gage daily precipitation record (Schumacher et al., 2018).

$$\text{Median BSI} \sim \text{Year} \times \text{Grazing} + \text{Precipitation} \quad (3)$$

This model tested whether the temporal trajectory of surface bareness differed among grazing histories, while adjusting for interannual variation in precipitation.

2.2 Project-scale monitoring

The specific goals of restoration structures installed at SPLT are varied, including controlling surface erosion, enhancing surface and subsurface water storage, and creating habitat. We broadly classified those placed in ephemeral channels as erosion control structures, as they shared a common mechanism aimed at increasing channel roughness and reducing flow velocity in backwater areas, thereby attenuating fluxes of sediment, water, wood, and other organic matter. In this analysis, in-channel erosion control and restoration structures were considered distinct only if they address separate problems spanning separate geomorphic contexts. For example, two one-rock dams placed in close proximity beneath the same piping-collapse headcut were grouped as a single structure, whereas two in the same vicinity but associated with distinct headcuts were treated separately.

Using this classification, SPLT installed three beaver dam analogs (BDAs), 24 log-based structures such as post-assisted log structures (PALS) and log step falls, and 65 rock-based structures including one-rock dams (ORDs) and Zuni bowls, for a total of 92 in-channel structures. Structure locations are shown in Figure 2. Of these, 51 were installed within Heartland Ranch Preserve and 42 within Raven's Nest. Only the three BDAs fell within the intermittent to perennial arroyo process domain; the 89 remaining structures were all placed in the ephemeral headwaters.

I documented the type, location, and condition of all distinct stream restoration structures across the study area (n = 92) using a qualitative field assessment. Structures were first categorized by intactness. For those that were intact, I recorded evidence of geomorphic change.

Deposition upstream of and within the interstitial spaces of the structures were the most commonly observed geomorphic changes, although avulsion around and scour downstream of structures were also observed. Unlike prior studies in similar semiarid regions that used depositional records from engineered sediment retention basins and erosion-control structures to estimate sediment load, I could not directly estimate the load because the LTPBR structures investigated here were less impervious than retention basins and were often destroyed, leaving an incomplete depositional record (Phippen & Wohl, 2003).

Accordingly, I classified structures into three categories: (1) not intact, (2) intact but ineffective, resulting in no detectable geomorphic change, and (3) intact and effective, resulting in geomorphic change. Examples of each outcome across different structure designs are shown in Figures 5–8. Structures categorized as "ineffective" because of their lack of detectable geomorphic response may still provide functional value by reducing flow velocity and damping energy.

Figure 5. Categorization of rock-based erosion control structure outcomes. Blue arrows indicate flow direction.

One-rock dams (ORDs) are installed perpendicular to flow and constructed, as the name suggests, as one-rock-high features made from locally sourced cobble to small boulder-sized clasts (Figure 5). Figure 5a shows an ORD destroyed during a high-flow event. Figure 5b shows an intact but ineffective ORD, with no sediment deposition in interstitial spaces. Figure 5c shows an effective ORD, where fine-grained fluvial sediment has accumulated within the interstitial spaces between rocks.

Figure 6: Categorization of log-based erosion control structure outcomes. Blue arrows indicate flow direction.

Post-assisted log structures (PALS) can take many forms; at SPLT, they typically feature small vertical stacks of logs or wooden fence posts, secured by posts driven into the channel bed (Figure 6). Figure 6a shows a PALS destroyed during a high-flow event, with only the posts remaining intact. Figure 6b shows an intact but ineffective log structure, trapping windblown vegetation but little sediment. Figure 6c shows an effective log structure, with fluvial sediment deposition visible upstream of the structure.

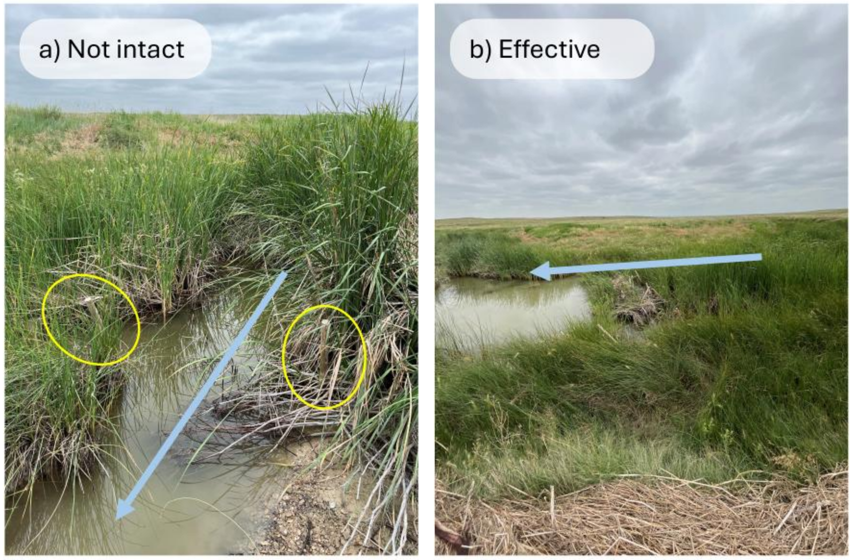

Figure 7: Categorization of beaver dam analog (BDA) outcomes. Blue arrows indicate flow direction.

Beaver dam analogs (BDAs) are typically constructed from packed mud, wood, and other organic material (Figure 7). Figure 7a shows a BDA destroyed during a high-flow event, with only the posts remaining intact. Figure 7b shows an effective BDA, with extensive upstream fine sediment deposition and cattail growth.

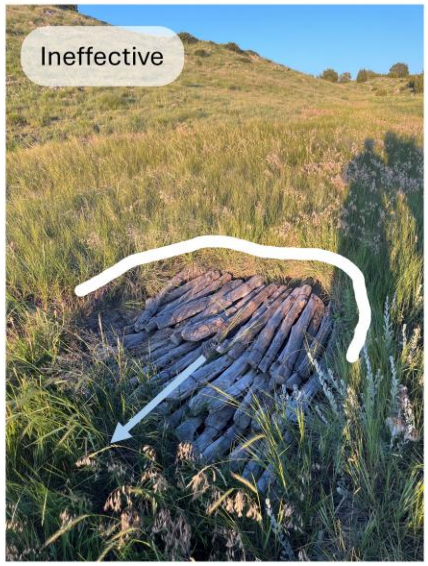

Figure 8: Ineffective log step-fall structure. White outline indicates approximate piping-collapse headcut scarp; blue arrow indicates flow direction.

Placed within a piping collapse, the log step-fall structure shown in Figure 8 fails to address a subsurface-driven erosion process with surface-based treatment. The absence of deposition within or upstream of the structure indicates that it does not interact with surface flow or fluvial sediment transport; rather, the logs simply cover evidence of the surrounding depression caused by subsurface erosion.

For each structure, I measured the surrounding bank angle using a laser range finder from the bed's break in slope to the top of the adjacent alluvial surface. I recorded local bank vegetation cover (foliar cover), classified as bare (<10% cover), sparse (10–50%), or heavy (>50%), and noted whether the structure was within three channel widths of a headcut. Whether a result of piping collapse or surface erosion, headcuts may serve as a point source of sediment that could influence structure outcomes. I initially considered recording proximity to roads, but only three structures had roads upstream that were close enough to contribute sediment under discontinuous flow conditions. I also considered including a variable indicating whether each structure was broadly associated with piping but excluded it from analysis, as it did not account for the many cases where depressions originally formed by piping collapse had since been modified by surface flow. Drainage area more effectively represented the relative influence of subsurface versus surface-driven erosion; headwaters streams with small drainage areas were dominated by piping collapse, whereas areas farther downstream with larger drainage areas were also influenced by surface flow. The specific effects of drainage area are discussed further in Results.

I calculated the catchment area upstream of each structure using a 1-m LiDAR-derived DEM and the *whitebox* package in R (Lindsay, 2016; Wu & Brown, 2022). From the same DEM, I calculated local slope as the average slope over a 10-m upstream distance (Hijmans, 2025). Local slope and vegetation cover are more relevant to project-scale outcomes than basin-wide averages because flows are often spatially discontinuous. The Revised Universal Soil Loss Equation (RUSLE) K-factor represents soil erodibility, and I extracted it from the NRCS Web Soil Survey for each restoration structure location (Renard et al., 2017; Soil Survey Staff, 2025). Finally, I recorded local grazing history within ~10 m of each structure (historic vs. recent commercial grazing). This variable was strongly associated with the year of installation, as the oldest structures were typically located in areas SPLT acquired and destocked earliest. Grazing history thus also serves as an indicator of structure age. In parcels with historic commercial grazing, most structures were installed during 2021 and 2022, with a few installed as early as 2017. In recently grazed areas, installations occurred after 2022, mostly in 2024.

To understand the factors contributing to the success or failure of restoration structures, I used a multivariate logistic regression model with the odds of intactness as the response variable and bank angle, bank vegetation cover, grazing history, soil erodibility, drainage area, local slope, and proximity to a headcut (Y/N) as predictors (4). I excluded the three BDAs from this analysis because their placement within the intermittent to perennial arroyo process domain required distinct measurement and analytical techniques from those used for structures in the ephemeral headwaters.

$$\text{Odds of intact structure} \sim \text{Bank angle} + \text{Bank vegetation cover} + \text{Grazing} + \text{K-factor} + \text{Drainage area} + \text{Local slope} + \text{Headcut indicator} \quad (4)$$

Because drainage area was the only significant predictor, I refitted a simpler univariate model with drainage area as the sole predictor (5).

$$\text{Odds of intact structure} \sim \text{Drainage area} \quad (5)$$

I compared the multivariate and univariate models using Akaike's Information Criterion (AIC), which balances model performance against model complexity (Akaike, 1973). The univariate model had a lower AIC score and was therefore selected for further statistical analysis.

Among intact structures, I fit a similar logistic regression model to determine the relative importance of factors contributing to whether a structure produced geomorphic change. This model (6) had the lowest AIC score among comparable models.

$$\text{Odds that intact structure results in geomorphic change} \sim \text{Bank angle} + \text{Bank vegetation cover} + \text{Grazing} + \text{K-factor} + \text{Drainage area} + \text{Local slope} + \text{Headcut indicator} \quad (6)$$

Because the BDAs produced pronounced and persistent backwater effects and deep pools, I surveyed longitudinal and cross-sectional profiles to qualitatively assess how they altered bed conditions and how site geomorphology contributed to their success or failure.

3. Results

3.1 Landscape-scale analysis

3.1.1 Soil compaction

As per the model presented in Equation (1), soil bulk density (ρ_b) is significantly higher in parcels with recent commercial cattle grazing (>0.115 AUM ha^{-1}) compared to parcels with light (~0.01 AUM ha^{-1}) bison/cattle pressure, controlling for background soil texture ($p<0.0001$). Figure 9 depicts the measured bulk density distribution across parcels A-F.

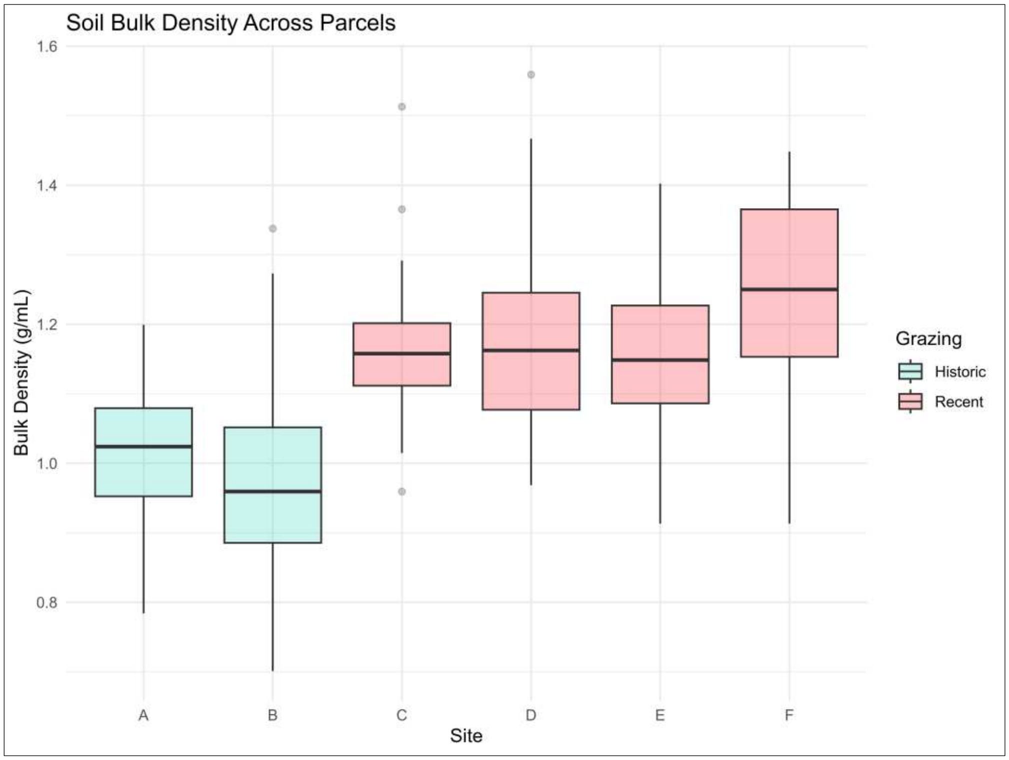

Figure 9: Measured soil bulk density (g/mL) across different parcels within SPLT's Heartland Preserve. Parcels with recent heavy cattle grazing are shown in red, and those with historic grazing in blue.

The grazing history-dependent relationship is consistent across all soil textures. Measured bulk densities are within commonly observed ranges as reported by McKenzie et al. (2002).

Table 2 shows the results of a contrast t-test on estimated marginal means, which tests whether soil bulk density in parcels without recent commercial grazing (A, B) differs from those with recent heavy grazing (C, D, E, F) within each soil-texture class. Positive contrast values indicate that recently grazed parcels have higher soil bulk density, i.e., greater compaction.

Table 2: Results for a contrast t-test on estimated marginal means, testing whether the soil bulk density (ρ_b) of parcels with recent commercial grazing differs from those without recent commercial grazing, within each soil-texture class.

Soil Texture (% sand)	Contrast in ρ_b (g/mL) by grazing history	95% CI (g/mL)	p-value
0-20%	0.179	(0.125, 0.233)	<0.0001
20-40%	0.153	(0.099, 0.208)	<0.0001
40-60%	0.232	(0.177, 0.288)	<0.0001
60-80%	0.192	(0.137,0.247)	<0.0001
Blue: significant, positive	Red: significant, negative		

Regardless of the underlying soil composition, recently grazed parcels are more compacted. The two sandiest classes exhibited the highest change in compaction (

Table 2). Sandy soils within the Heartland Ranch Preserve are typically found on hilltops and exhibit shallower soil profiles than the finer soils found in valley bottoms. Orodho et al. (1990) observed similar grazing-induced compaction in New Mexico and posited that shallow hilltop soils may be more impacted than deeper valley-bottom soils (Trimble & Mendel, 1995); my findings are consistent with this observation. Overall, these results support Hypothesis 1a and suggest that grazing history is a strong predictor of soil bulk density.

3.1.2 Vegetation cover

The BSI distribution across Heartland Ranch Preserve for the 2024 growing season composite Landsat image is shown in Figure 10.

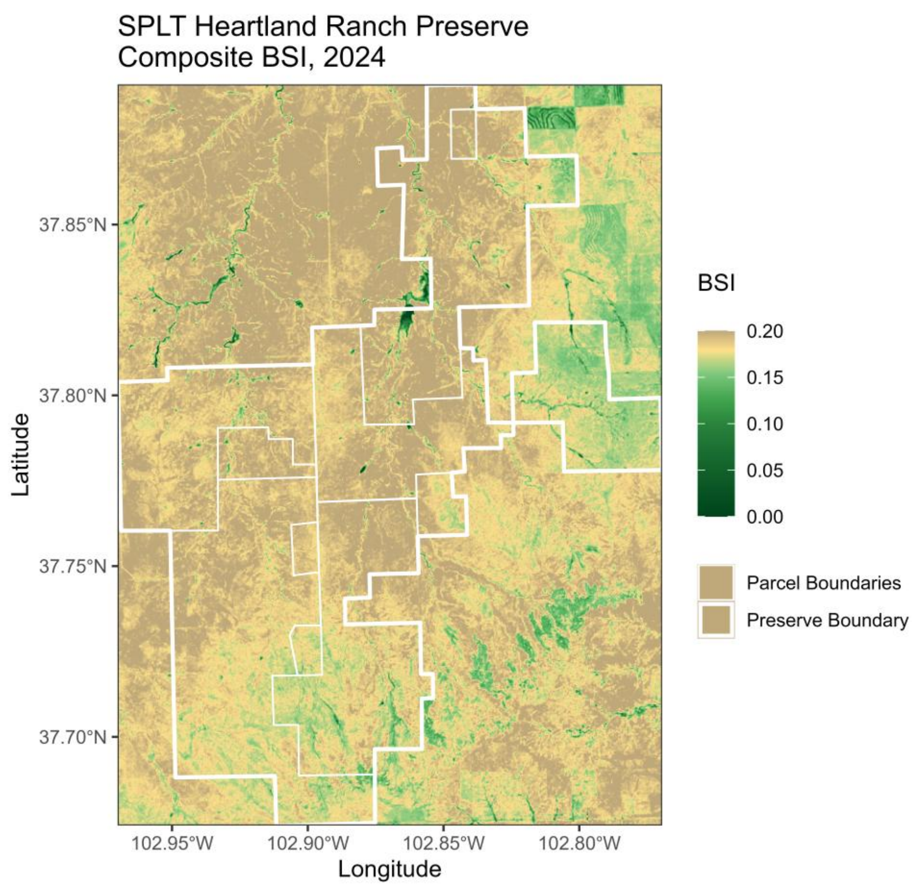

Figure 10: Bare soil index (BSI) across SPLT's Heartland Ranch Preserve, from a 2024 growing season Landsat composite image.

High BSI values indicate greater soil bareness, or lower vegetation cover. The headwaters region just downstream of the mesa, in the southeastern corner of the area shown in Figure 10, forms an arc of relatively dense vegetation. Field observations of comparatively lush vegetation and ephemeral wetlands north of the mesa are consistent with this remotely sensed observation; a photograph of this area is shown in Figure 1a. Other zones of dense vegetation occur along channels with perennial flow in the north-central part of the region, as well as around isolated groundwater springs and agricultural fields. In contrast, much of the northern half of the preserve exhibits relatively bare conditions.

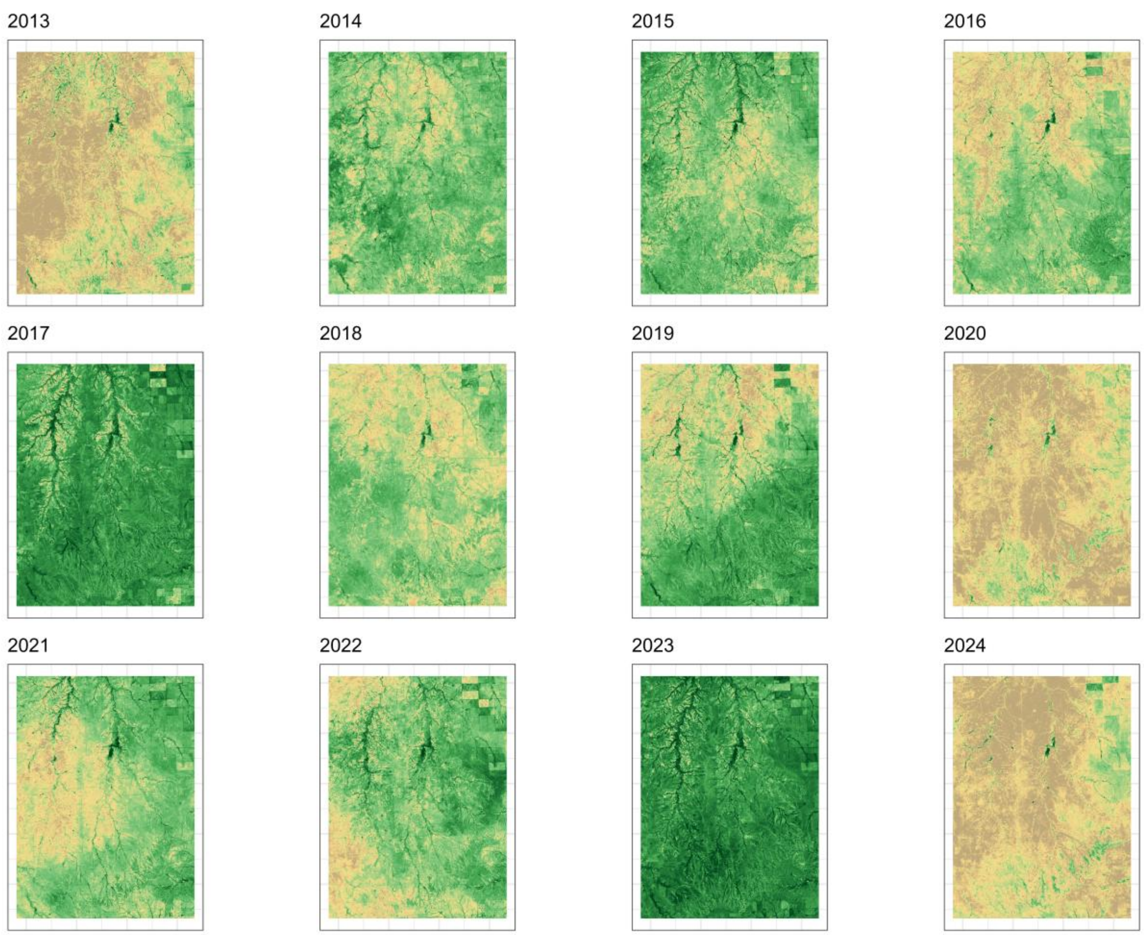

Figure 11: Composite growing season bare soil index (BSI) across SPLT's Heartland Ranch Preserve, 2013-2024.

Similar BSI spatial patterns are seen in 2013 and 2020 (Figure 11). The clearest trend, however, when examining the temporal trajectory of growing-season composite BSI, is that BSI varies substantially through time, with some years showing markedly higher vegetation cover. This pattern is expected, as vegetation in semiarid ecosystems is highly dependent on precipitation, which itself exhibits strong interannual variability driven by the North American Monsoon, the distribution of regional and mesoscale precipitation events and localized convective storms. To account for this variability, I included precipitation as a covariate in the model presented in Equation (3). The trajectory of soil bareness through time is not dependent on grazing history but is strongly and inversely associated with growing-season precipitation ($p < 0.0001$). These results do not support Hypothesis 1b and suggest that recent grazing management has not had a significant effect on vegetation cover.

3.2 Project-scale monitoring

Restoration structure outcomes across the SPLT's Heartland Ranch and Raven's Nest Preserves are shown in Figure 12i-iv. In total, 22 (24%) erosion control (e.g., Zeedyk structures, PALS) structures were destroyed, 42 (46%) were intact but resulted in no detectable geomorphic change and 28 (30%) were intact and geomorphically responsive. One of the three distinct BDAs (33%) was destroyed, the other two (67%) were intact and geomorphically effective.

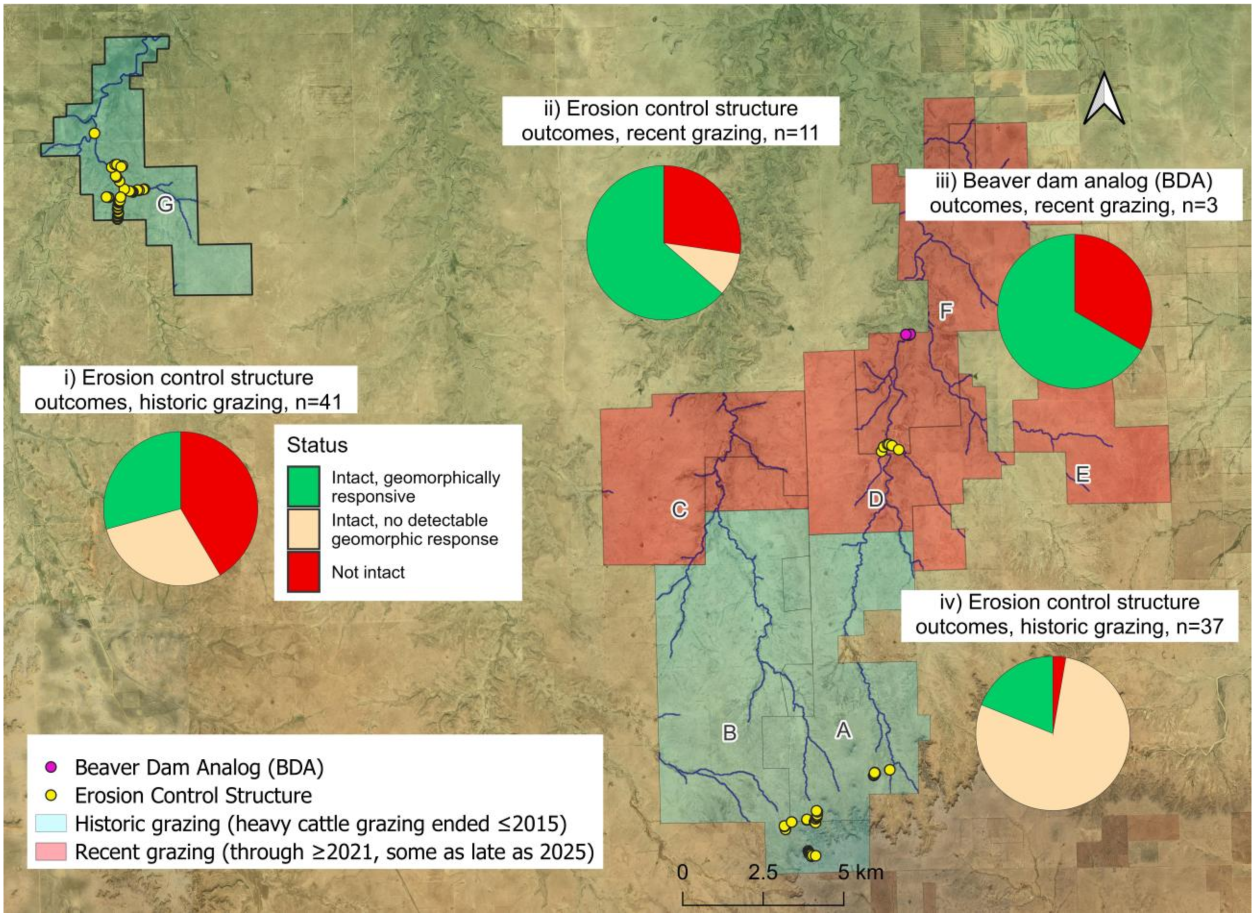

Figure 12: Erosion control and beaver dam analog (BDA) outcomes across different geomorphic settings (i-iv). Parcels labeled as A-G.

The spatial distribution of structure outcomes shown in Figure 12 reveals a clear drainage-area control, with structures located in the headwaters just north of the mesa mostly intact but producing little geomorphic change. Farther downstream, fewer structures remain intact, but more have trapped sediment, resulting in their classification as effective. Grazing history also appears to influence restoration outcomes: structures on Raven's Nest Preserve (Figure 12i) were less effective than those in downstream portions of Heartland Ranch (Figure 12ii), despite similar positions within the drainage network and an older installation date (2021-2022). The structures in Figure 12ii were installed in more recently grazed areas and have had less time (since 2024) to interact with flows.

This trend is confirmed in an analysis of the results from the multivariate logistic regression models presented in Equations (5) and (6). Each additional km^2 of drainage area is associated with, on average, 6.6% lower odds of structure intactness ($p<0.0001$). Conversely, among intact structures, each additional km^2 of drainage area is associated with, on average, 11% higher odds of geomorphic change ($p=1.49\times 10^{-3}$).

The results of the multivariate logistic regression model presented in Equation (6) are shown in Table 3. Some logistic regression odds ratios are extreme with wide confidence intervals, particularly the ratio associated with slope, because a one-unit change in slope is far larger than the observed range (roughly 0-0.1). Extreme values may also reflect a small sample size (n=92) and multicollinearity. Aside from drainage area, higher local slope, sparse (<50%) bank vegetation cover, and recent commercial grazing each increased the odds that an intact structure produced geomorphic change, when controlling for all other variables in the model (Table 3).

Table 3: Outcomes of multivariate logistic binary regression analysis, examining the influence of various basin and local characteristics on the odds that an erosion control structure resulted in geomorphic change.

Predictor	Odds Ratio	95% CI	p-value
Drainage area (km^2)	1.11	(1.05, 1.19)	1.49×10^{-3}
Local Slope (m/m)	5.45×10^{15}	(1.91×10^{3}, 6.70×10^{32})	4.37×10^{-2}
Bank Angle (degrees)	0.991	(0.948, 1.03)	0.665
RUSLE K-factor	7.56	(5.40×10^{-3}, 1.32×10^{4})	0.582
Recent Grazing (vs historic)	32.2	(2.63, 1.14×10^{3})	1.84×10^{-2}
Near headcut (vs not)	9.64×10^{-2}	(6.07×10^{-3}, 0.783)	5.43×10^{-2}
Bare bank vegetation (vs heavy)	42.5	(1.90, 2.47×10^{3})	3.51×10^{-2}
Sparse bank vegetation (vs heavy)	0.996	(0.141, 6.08)	0.996
Blue: significant, >1	Red: significant, <1		

The competing effect of drainage area on restoration outcomes is shown in Figure 13, which plots the odds of structure intactness and structure-induced geomorphic change versus drainage area. Structure intactness decreases exponentially but structure-induced geomorphic change increases exponentially with increasing drainage area. The large uncertainty band associated with the geomorphic change line reflects the additional controls exerted by slope, bank vegetation and grazing history, whereas intactness is primarily a function of drainage area.

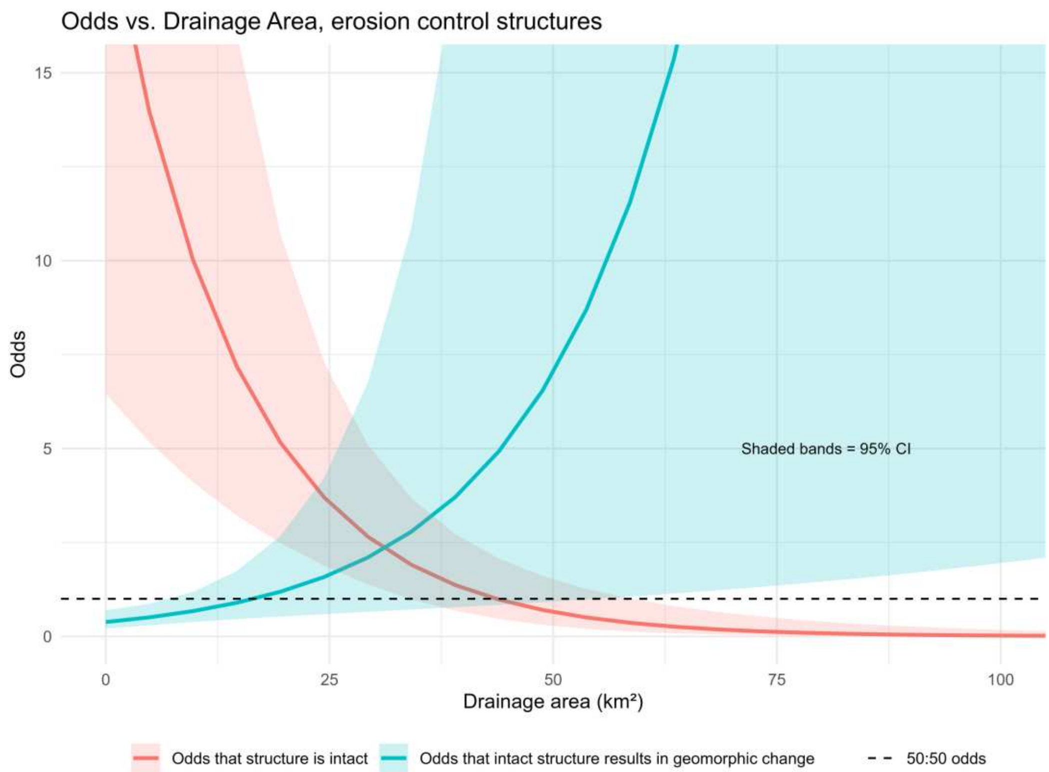

Figure 13: Odds of erosion control structure intactness (red) and structure-induced geomorphic change (blue) as a function of drainage area (km²). Shaded regions show 95% confidence bands. A dashed black line indicates 50:50 odds.

The small BDA sample size (n = 3) makes statistical modeling ineffective for identifying factors contributing to restoration outcomes. All three BDAs were installed along a deeply incised, low-gradient section of Mud Creek with perennial flow and an upstream catchment area of ~82 km². The valley bottom here is densely vegetated with cattails, sedges, and grasses, and all sites fall within the "recent" commercial grazing regime (Figure 7). Two BDAs remained intact and produced extensive upstream backwater and fine sediment deposition, while the third failed. The failed structure was located in a slightly more confined reach with a steeper average bank angle (21°) compared to ~10° for the successful BDAs. This confinement likely increased flow depth and velocity during high flows, amplifying the shear and normal stresses on the structure that ultimately contributed to its destruction.

These results support Hypothesis 2a in that, within the ephemeral headwaters, structures placed higher in the catchment—within piping-dominated areas of low drainage area—were unlikely to produce geomorphic change. In contrast, structures located farther downstream in zones of episodic surface flow were more likely to capture material, particularly where gradients were high and vegetation was sparse. These results also support Hypothesis 2b, indicating that the success of BDAs depended primarily on bank morphology, namely bank angle and degree of confinement.

4. Discussion

4.1 Landscape-scale recovery

Upland response to cattle grazing is not uniform. Bulk density responded within ten years, as indicated by consistent differences in bulk density in relation to grazing history. Although parcels C–F differ slightly in acquisition history and cattle were removed at various times between 2021 and 2025, all still exhibit elevated bulk density compared to parcels A and B, which have experienced only light, non-commercial, bison-dominated grazing since 2015 (Figure 9). This suggests that the threshold for measurable recovery of soil structure in this semiarid grassland system exceeds four years and is likely on the order of a decade. Consistent with this interpretation, previous studies of hydrologic recovery in Colorado grasslands found that infiltration rates required roughly 13 years to return to pre-disturbance levels (Dortignac & Love, 1961; Branson et al., 1981).

In contrast, vegetation cover did not respond within ten years of cessation of cattle grazing. A growing body of literature indicates that, at landscape scales, even intensive rotational or other managed grazing systems may not produce significant increases in vegetation cover relative to non-rotational practices (Briske et al., 2008; Hawkins, 2017; Venter et al., 2019). While grazing management at SPLT is not rotational but rather represents a step reduction in stocking rate, the underlying principle is similar: remove livestock to allow vegetation to recover. The BSI signal, however, implies high vegetation cover during wet years but no difference in the grazed versus ungrazed temporal soil bareness trajectory after accounting for background precipitation. This trend suggests that interannual changes in remotely sensed ground cover are dominated by annual plant growth or background soil moisture rather than persistent increases in perennial cover following grazing reduction.

Several explanations may account for the observed similarity in vegetation cover among parcels with different grazing histories. One possibility is that grazing occurred below the landscape's carrying capacity and therefore did not significantly affect vegetation cover. Work in South African rangelands has suggested that comparable vegetation cover under both continuous and rotational management indicates grazing occurred below carrying capacity (Venter et al., 2019). A second possibility is that vegetation cover was diminished long ago and has not yet recovered. Given the long (>100 yr) commercial grazing history at SPLT and the ubiquity of grazing in adjacent areas, pre-grazing conditions are unknown and the complete grazing chronology is uncertain beyond the years immediately prior to acquisition by SPLT. It is therefore possible that the similarity in vegetation cover relative to recently grazed parcels instead reflects a lack of recovery. Mechanistically, desiccation cracking provides a plausible explanation for this persistent legacy: field experiments have shown that in shrink-swell clay soils like those at SPLT, grazing-induced structural damage promotes extensive cracking, whereas ungrazed soils experience shrink-swell cycles without surface rupture (Reid & Parkinson, 1984). Once cracks form, precipitation infiltrates rapidly through the topsoil into deeper layers, potentially preventing vegetation recovery for decades and perpetuating the legacy of historic grazing (Reid & Parkinson, 1984).

A third possibility is that vegetation recovery is occurring, but at different timescales across the landscape. In the Great Basin, Fesenmyer et al. (2018) documented increases in remotely sensed riparian vegetation condition (NDVI) within three years of implementing grazing exclosures and conservation-oriented grazing. Recovery in those systems was measured near channels and dominated by woody species such as willow, often facilitated by subsequent beaver colonization and dam-building activity. Although the vegetation composition of the Great Basin differs markedly from that of the Great Plains, these results demonstrate that, in a semiarid environment, riparian vegetation recovery can occur relatively quickly under favorable grazing management. At SPLT, however, any such localized response is overshadowed by the absence of measurable change in grassland vegetation across the broader landscape, which appears to be changing on timescales longer than have been observed thus far following grazing cessation.

Further, perennial grass recovery in semiarid uplands may manifest as changes in root biomass, basal cover, or changes in species composition—none of which are detectable by BSI. The BSI analysis here indicates that, on a landscape scale, there is no large-scale signal of year-to-year aboveground recovery after controlling for precipitation. The remote methods used here likely did not capture recovery at the patch, plant, riparian, or subsurface scales.

4.2 Project-scale outcomes

In small drainage areas, erosion is dominated by subsurface piping collapse, so restoration structures typically remain intact but experience little surface flow to transport sediment. This is because they are often located on valley floors, in channels with infrequent or limited surface flow, or just upstream of piping collapses, where runoff is insufficient to mobilize sediment. Structures were rarely sited just downstream of collapse locations, even though this position could intercept sediment loads during ephemeral flows. In larger drainage areas, erosion results from the combined effects of subsurface piping and surface processes, and while piping still occurs, collapses are more frequently reworked and redistributed by in-channel surface flows. In channels with large contributing areas, flash floods may destroy structures, yet those that remain intact may trap sediment, particularly in steep, sparsely vegetated, and recently grazed reaches (Figure 13; Table 3). Essentially, structures are most geomorphically responsive where they intercept high sediment loads. This relationship aligns with prior studies showing that steep, sparsely vegetated reaches in semiarid landscapes contribute disproportionately to sediment flux and that hard-engineered erosion control efforts are often ineffective when these fundamental drivers are overlooked (Marston & Dolan, 1999; Phippen & Wohl, 2003). The outcomes of LTPBR, Zeedyk, and NIDS structures are no different; the geomorphic response is governed primarily by context rather than intervention type (Wohl et al., 2024).

The influence of grazing history on restoration outcomes suggests a nonlinear, two-phase recovery trajectory analogous to those observed following dam removal, large floods, and other disturbances (Pizzuto, 2002; Fields et al., 2025). I follow Fields et al.'s (2025) application of Schumm's (1973, 1979) concepts of intrinsic and extrinsic geomorphic thresholds in defining these two phases. The first phase, operating over short timescales, involves rapid adjustment of intrinsic channel properties—such as width, depth, and grain size at the transect scale—to prevailing hydrologic conditions (i.e., flows within bankfull). The second phase, occurring over longer timescales, involves adjustments of extrinsic properties at the reach-to-landscape scale, including hillslope morphology and sediment-supply processes (e.g., piping, surface erosion) that are driven by changing boundary conditions such as land use, extreme flows, climate, subsidence, uplift, and geology (Fields et al., 2025; Schumm, 1973; Schumm, 1979). While the concept of a "bankfull" channel is less applicable in incised arroyo systems, the overall framework captures the dynamics of recovery.

Despite comparable positions within the catchment and later installation, structures in the recently grazed northern portion of Heartland Ranch Preserve were more likely to exhibit geomorphic change (64%) than those at Raven's Nest Preserve (29%; Figure 12i-ii). Most structures within Heartland's northern parcels were installed in 2024, shortly after the end of commercial grazing in 2023. Residual soil compaction and subsequent surface erosion at these sites allowed ordinary flows to mobilize and deposit sediment, temporarily lowering the effective precipitation and effective discharge (Wolman & Miller, 1960; Schumm, 1979). The deposits behind restoration structures therefore reflect transect-scale channel adjustment rapidly modulated by the prevailing hydrology.

I infer that ordinary flows no longer produce significant sediment transport to the structures over longer timescales. In long-rested areas, adjustment is governed primarily by extrinsic alterations to boundary conditions beyond the channel, driven by land use, climate, vegetation, and extreme events rather than by ordinary flows (Fields et al., 2025). In this system, relevant extrinsic controls include the reduction of soil compaction through time (Figure 9), which limits overland flow and surface erosion, and episodic large floods capable of destroying restoration structures. Most structures at Raven's Nest Preserve were installed during 2021–2022, long after the end of commercial grazing in 2013. Consequently, the higher proportion of destroyed structures (41%) and the lower proportion that produced geomorphic change (29%) at Raven's Nest likely reflect this shift to a lower-compaction, low-sediment, flood-driven recovery regime rather than a difference in design efficacy (Figure 12i).

Finally, these findings raise a broader question: to what extent can structure-based restoration in grassland systems be considered truly process-based? In this study, only about 30% of LTPBR, NIDS, and Zeedyk-style erosion-control structures were both intact and produced detectable geomorphic change. The philosophy behind LTPBR recognizes the potential for multiple drivers of stream degradation (Wheaton et al., 2019). However, as commonly implemented, LTPBR assumes that the dominant process disruption is a decline in the spatial frequency of natural in-channel obstacles to flow resulting from large wood loss, channel straightening, and beaver extirpation (Beardsley, 2024), or so-called structural starvation. Structural starvation is a common impairment, and where this assumption holds, process-based restoration should focus on re-establishing persistent, self-sustaining log jams, beaver dams, and other sources of in-channel heterogeneity. However, in fine-grained, wood-poor grassland systems, one-rock dams, Zuni bowls, PALS, and log step-falls do not reflect forms that are naturally generated or sustained by local geomorphic processes. Although some restoration manuals acknowledge that structural starvation is not universal (Wheaton et al., 2019), the widespread appeal of LTPBR has encouraged a one-size-fits-all approach that often overlooks the processes governing channel adjustment (Nash et al., 2021; Wohl et al., 2024).

4.3 Restoration decision framework

Based on my field observations and data analyses at the Southern Plains Land Trust preserves, I developed a decision framework that can be used to evaluate the potential efficacy of future restoration structures when sites and methods of stream restoration are being considered (Table 4). The quantitative thresholds for drainage area and time since grazing ceased are specific to this field area, but the general approach should be applicable to other semiarid grasslands that exhibit both piping and surface erosion as sources of channel formation and modification. In other words, comparable frameworks could be developed for other semiarid grasslands, recognizing that specific numeric thresholds will vary with topography, hydrology, geology, soil texture, vegetation, land use, and disturbance history.

Table 4: Southern Plains Land Trust stream restoration decision framework.

Southern Plains Land Trust stream restoration decision framework
(1) Is there a specific management problem caused by a physical process? No: Do not install in-channel structural interventions. Yes: Go to (2).
(2) Is there active grazing or another land use disturbance resulting in compaction, reduced vegetation cover & elevated sediment yield (e.g., roads, drill pads)? No: Go to (4). Yes: Go to (3).
(3) Can you address the underlying cause of the compaction disturbance (e.g., remove cows, decommission and rip roads)? No: Do not install in-channel structural interventions. Structures are not self-sustaining, and an ongoing land use disturbance may quickly deplete structural sediment storage. Structures only temporarily alleviate symptoms if the disturbance is ongoing. Yes: Address disturbance, return to (1).
(4) Is drainage area <16 km^2 and is geomorphic change dominated by subsurface soil piping collapse? No: Go to (5). Yes: Do not install in-channel structural interventions. Surface structures do not prevent subsurface-driven erosion and are ineffective at stabilizing such headcuts; they should not be installed in close proximity to them. Instead, structures are better suited to portions of the channel dominated by surface flow and located sufficiently far

downstream from active headcuts, where they can enhance natural bank angle reduction and vegetation recolonization.

(5) Is drainage area >44 km^2 (large discharge, high shear stress)?

No: Go to (7).

Yes: Erosion-control structures (e.g., PALS, ORDs, Zuni bowls etc.) are unlikely to stay intact. Go to (6).

(6) Is there perennial flow?

No: Do not install in-channel structural interventions.

Yes: If banks are shallow (~10°) and vegetation has heavily encroached into the already-widening arroyo channel (Schumm et al., 1984), BDAs may enhance natural stabilization and promote additional water storage and vegetation growth.

(7) Did the compaction disturbance end ≤10 years ago?

No: Do not install in-channel structural interventions. Bulk density and infiltration have likely recovered and there is less disturbance-enhanced erosion and sediment yield.

Yes: Consider structural intervention, while recognizing that coarse material and large-wood analogs are not likely to be self-sustaining and may not align with the dominant geomorphic processes operating in grasslands stream corridors. Target areas with high sediment yield; these may be areas with relatively high slopes and low local vegetation cover.

The decision steps in Table 4 reflect my observations that, in the study area, (i) structural interventions in close proximity to an active headcut generated by piping are not effective and (ii) erosion-control structures are unlikely to remain intact in ephemeral channels with large contributing areas.

5. Conclusions

In this chapter, I conducted multiscale monitoring of post-grazing recovery and restoration outcomes in semiarid grassland headwater channels, spanning transect to landscape scales. The Mud and Rule Creek catchments and adjacent land managed by the Southern Plains Land Trust (SPLT) in southeastern Colorado served as a case study for this work, although the general patterns observed are likely representative of similar semiarid grassland systems elsewhere. I examined landscape-scale recovery of soil compaction and vegetation cover following cattle removal, finding that the two are out of sync. Soil bulk density was significantly lower in parcels that had rested for roughly a decade compared to those rested for less than five years, whereas changes in remotely sensed upland vegetation cover were comparable among grazing histories.

I also evaluated the geomorphic factors controlling the intactness and geomorphic effectiveness of in-channel restoration structures (LTPBR, NIDS, and Zeedyk), finding that success depends strongly on geomorphic context. In channels draining small catchments, erosion is dominated by subsurface piping collapse; structures typically remain intact but trap little sediment because surface flow is minimal. In larger catchments, flash floods may destroy some structures, but those that remain intact are more likely to trap sediment—especially in steep, sparsely vegetated, and recently grazed reaches. Thus, structure intactness primarily reflects the flow regime, while the geomorphic impacts of in-channel restoration structures primarily reflect local sediment supply.

I hypothesize that post-grazing recovery follows a nonlinear trajectory, beginning with an early phase of event-to-annual timescale reworking of sediment delivered to channels from recently grazed, still-compacted hillslopes during regular low-flow and small-runoff events in ephemeral channels. This gives way to longer-term, decadal-scale adjustments across the broader landscape driven by soil recovery (decompaction) and episodic high-magnitude storm events. To guide future restoration efforts at SPLT, I developed a simple dichotomous key that could be adapted for other semiarid grassland systems. As in any landscape, truly process-based restoration must identify and address the geomorphic processes driving channel adjustment, whether soil piping, surface erosion, or beaver activity, rather than rely on generic structural templates.

References

Akaike, H. (1998). Information theory and an extension of the maximum likelihood principle. In *Selected papers of Hirotugu Akaike* (pp. 199-213). New York, NY: Springer New York.

Beardsley, M. (2024). *A perspective on the LTPBR phenomenon* [White paper]. ResearchGate. https://www.researchgate.net/publication/377967162_A_Perspective_on_the_LTPBR_Phenomenon

Beechie, T.J., Sear, D.A., Olden, J.D., Pess, G.R., Buffington, J.M., Moir, H., Roni, P., & Pollock, M. M. (2010). Process-based principles for restoring river ecosystems. *BioScience*, *60*(3), 209-222.

Bergstrom, J. C., & Loomis, J. B. (2017). Economic valuation of river restoration: An analysis of the valuation literature and its uses in decision-making. *Water Resources and Economics*, *17*, 9-19.

Bernhardt, E.S., Palmer, M.A., Allan, J.D., Alexander, G., Barnas, K., Brooks, S., Carr, J., Clayton, S., Dahm, C., Follstad-Shah, J., & Sudduth, E. (2005). Synthesizing US river restoration efforts. *Science*, *308*(5722), 636-637.

Blackburn, W. H., & Skau, C. M. (1974). Infiltration rates and sediment production of selected plant communities in Nevada. *Rangeland Ecology & Management/Journal of Range Management Archives*, *27*(6), 476-480.

Branson, F. A., Gifford, G. F., Renard, K. G., & Hadley, R. F. (1981). *Rangeland Hydrology*. Kendall/Hunt.

Briske, D.D., Derner, J.D., Brown, J.R., Fuhlendorf, S.D., Teague, W.R., Havstad, K.M., Gillen, R.L., Ash, A.J., & Willms, W. D. (2008). Rotational grazing on rangelands:

reconciliation of perception and experimental evidence. *Rangeland Ecology & Management*, *61*(1), 3-17.

Dortignac, E. J., & Love, L. D. (1961). *Infiltration studies on ponderosa pine ranges of Colorado*. Publications of the Rocky Mountain Forest and Range Experiment Station. U.S. Department of Agriculture, Forest Service.

Dortignac, E. J., & Hickey, W. C. (1963). *Surface runoff and erosion as affected by soil ripping*. US Department of Agriculture, Forest Service.

Fesenmyer, K. A., Dauwalter, D. C., Evans, C., & Allai, T. (2018). Livestock management, beaver, and climate influences on riparian vegetation in a semi-arid landscape. *PLoS One*, *13*(12), e0208928.

Fields, J. F., Renshaw, C. E., Dethier, E. N., & Magilligan, F. J. (2025). The longer arc of channel recovery post-dam removal. *Geomorphology*, *468*, 109442.

Floyd, E. J. (1974). Tunnel erosion: A field study in the Riverina, New South Wales. *Journal of the Soil Conservation Service of New South Wales, 30*(3), 145–156.

Ganskopp, D. (2001). Manipulating cattle distribution with salt and water in large arid-land pastures: a GPS/GIS assessment. *Applied Animal Behaviour Science*, *73*(4), 251-262.

Gellis, A. C., Cheama, A., Laahty, V., & Lalio, S. (1995). Assessment of gully-control structures in the Rio Nutria watershed, Zuni Reservation, New Mexico. *JAWRA Journal of the American Water Resources Association, 31*(4), 633–646.

Gellis, A. C., Cheama, A., & Lalio, S. M. (2001). Developing a geomorphic approach for ranking watersheds for rehabilitation, Zuni Indian Reservation, New Mexico. *Geomorphology*, *37*(1-2), 105-134.

Gorelick, N., Hancher, M., Dixon, M., Ilyushchenko, S., Thau, D., & Moore, R. (2017). Google Earth Engine: Planetary-scale geospatial analysis for everyone. *Remote Sensing of Environment*, *202*, 18-27.

Hawkins, H. J. (2017). A global assessment of Holistic Planned Grazing™ compared with season-long, continuous grazing: meta-analysis findings. *African Journal of Range & Forage Science*, *34*(2), 65-75.

Hijmans, R. (2025). *terra: Spatial data analysis* (Version 1.8-15) [R package]. https://CRAN.R-project.org/package=terra

Huang, S., Tang, L., Hupy, J. P., Wang, Y., & Shao, G. (2021). A commentary review on the use of normalized difference vegetation index (NDVI) in the era of popular remote sensing. *Journal of Forestry Research*, *32*(1), 1-6.

Larsen, A., Larsen, J. R., & Lane, S. N. (2021). Dam builders and their works: Beaver influences on the structure and function of river corridor hydrology, geomorphology, biogeochemistry and ecosystems. *Earth-Science Reviews*, *218*, 103623.

Lenth, R. (2025). *emmeans: Estimated marginal means, aka least-squares means* (R package version 1.10.7). https://CRAN.R-project.org/package=emmeans

Lillesand, T., Kiefer, R. W., & Chipman, J. (2015). *Remote Sensing and Image Interpretation*. John Wiley & Sons.

Lindsay, J. B. (2016). Whitebox GAT: A case study in geomorphometric analysis. *Computers & Geosciences, 95*, 75–84. https://doi.org/10.1016/j.cageo.2016.07.003

Maestas, J. D., Conner, S., Zeedyk, B., Neely, B., Rondeau, R., Seward, N., Chapman, T., & Murph, R. (2018). *Hand-built structures for restoring degraded meadows in sagebrush rangelands: Examples and lessons learned from the Upper Gunnison River Basin,* *Colorado* (Range Technical Note No. 40). U.S. Department of Agriculture, Natural Resources Conservation Service, Colorado.

Marston, R. A., & Dolan, L. S. (1999). Effectiveness of sediment control structures relative to spatial patterns of upland soil loss in an arid watershed, Wyoming. *Geomorphology*, *31*(1-4), 313-323.

McKenzie, N., Coughlan, K., & Cresswell, H. (2002). *Soil physical measurement and interpretation for land evaluation*. CSIRO Publishing.

Meeuwig, R. O. (1970). Infiltration and soil erosion as influenced by vegetation and soil in northern Utah. *Rangeland Ecology & Management/Journal of Range Management Archives*, *23*(3), 185-188.

Nash, C.S., Grant, G.E., Charnley, S., Dunham, J.B., Gosnell, H., Hausner, M.B., Pilliod, D.S., & Taylor, J. D. (2021). Great expectations: Deconstructing the process pathways underlying beaver-related restoration. *BioScience*, *71*(3), 249-267.

Norman, L. M., Lal, R., Wohl, E., Fairfax, E., Gellis, A. C., & Pollock, M. M. (2022). Natural infrastructure in dryland streams (NIDS) can establish regenerative wetland sinks that reverse desertification and strengthen climate resilience. *Science of the Total Environment*, *849*, 157738.

Orodho, A. B., Trlica, M. J., & Bonham, C. D. (1990). Long-term heavy-grazing effects on soil and vegetation in the four corners region. *The Southwestern Naturalist*, 9-14.

Patton, P. C., & Schumm, S. A. (1975). Gully erosion, Northwestern Colorado: a threshold phenomenon. *Geology*, *3*(2), 88-90.

Phippen, S. J., & Wohl, E. (2003). An assessment of land use and other factors affecting sediment loads in the Rio Puerco watershed, New Mexico. *Geomorphology*, *52*(3-4), 269-287.

Pizzuto, J. (2002). Effects of dam removal on river form and process. *BioScience*, *52*(8), 683–691.

Pollock, M. M., Beechie, T. J., Wheaton, J. M., Jordan, C. E., Bouwes, N., Weber, N., & Volk, C. (2014). Using beaver dams to restore incised stream ecosystems. *BioScience*, *64*(4), 279–290.

R Core Team. (2025). R: A language and environment for statistical computing. R Foundation for Statistical Computing, Vienna, Austria. *http://www. R-project. org/.*

Reid, I., & Parkinson, R. J. (1984). The wetting and drying of a grazed and ungrazed clay soil. *Journal of Soil Science*, *35*(4), 607–614.

Renard, K. G., Laflen, J. M., Foster, G. R., & McCool, D. K. (2017). The revised universal soil loss equation. In *Soil Erosion Research Methods* (pp. 105-126). Routledge.

Rikimaru, A., Roy, P. S., & Miyatake, S. (2002). Tropical forest cover density mapping. *Tropical Ecology*, *43*(1), 39-47.

Scamardo, J., Munger, W., Loria, K., Nauman, B., Wang, J., Leopold, S., Heggli, A., Huntly, N., Baker, M., & Meadow, A. M. (2025). Trends in the Outcomes, Practice, and Law of Low-Tech Process-Based Restoration in Western Rangelands. *Rangeland Ecology & Management*, *98*, 344-356.

Schumacher, R. S., Goble, P. E., Schwalbe, Z., & Bolinger, R. A. (2018). Using CoAgMET, “Colorado’s Mesonet,” to analyze our state’s weather and climate. *Colorado Water, 35*(5).

Schumm, S. A. (1973). Geomorphic thresholds and complex response of drainage systems. *Fluvial Geomorphology*, *6*, 69-85.

Schumm, S. A. (1979). Geomorphic thresholds: the concept and its applications. *Transactions of the Institute of British Geographers, 4,* 485-515.

Schumm, S. A., Harvey, M. D., & Watson, C. C. (1984). *Incised channels: Morphology, dynamics, and control.* Water Resources Publications.

Soil Survey Staff, Natural Resources Conservation Service, United States Department of Agriculture. (2025). *Web Soil Survey*. Retrieved March 15, 2025, from https://websoilsurvey.sc.egov.usda.gov/

Trimble, S. W., & Mendel, A. C. (1995). The cow as a geomorphic agent—a critical review. *Geomorphology*, *13*(1-4), 233–253.

Venter, Z. S., Cramer, M. D., & Hawkins, H. J. (2019). Rotational grazing management has little effect on remotely-sensed vegetation characteristics across farm fence-line contrasts. *Agriculture, Ecosystems & Environment*, *282*, 40–48.

Wheaton, J. M., Bennett, S. N., Bouwes, N., Maestas, J. D., & Shahverdian, S. M. (Eds.). (2019). *Low-tech process-based restoration of riverscapes: Design manual* (Version 1.0) [Manual]. Utah State University Restoration Consortium. https://doi.org/10.13140/RG.2.2.19590.63049/2

Wohl, E., Rathburn, S., Dunn, S., Iskin, E., Katz, A., Marshall, A., Means-Brous, M., Scamardo, J., Triantafillou, S., & Uno, H. (2024). Geomorphic context in process-based river restoration. *River Research and Applications*, *40*(3), 322-340.

Wolman, M. G., & Miller, J. P. (1960). Magnitude and frequency of forces in geomorphic processes. *The Journal of Geology*, *68*(1), 54-74.

Wu, Q., & Brown, A. (2022). *whitebox: "WhiteboxTools" R frontend* (Version 2.2.0) [R package]. https://CRAN.R-project.org/package=whitebox

Zeedyk, B., & Jansens, J.-W. (2009). *An introduction to erosion control* (3rd ed.). Earth Works Institute, the Quivira Coalition, and Zeedyk Ecological Consulting.

CHAPTER 3: HYDROLOGIC CONSTRAINTS ON SOIL PIPING INITIATION IN SEMIARID GRASSLANDS

1. Introduction

In the ephemeral headwaters of semiarid grassland streams, surface restoration techniques are ineffective at addressing erosion caused by the collapse of subsurface soil piping networks (Chapter 2). The natural follow-up is to investigate controls on piping initiation and mechanisms to improve our understanding of how land use and management may influence piping processes. Although soil piping and piping-collapse are natural components of hillslope systems worldwide and are often misunderstood in management contexts, they are increasingly recognized in the literature for their impacts on human society through their roles in rainfall-runoff relationships, the carbon cycle, biodiversity, and their geohazard potential (Bryan & Jones, 1997; Bernatek-Jakiel & Nadal-Romero, 2023). Together with pipeflow's contributions to stormflow—in some cases, upwards of 50% of stormflow discharge—this recognition has prompted efforts to model soil piping processes across scales, from local initiation to catchment response (Swanson et al., 1989; Jones, 2010).

1.1 Physical and numerical models of piping processes

Piping is a dominant mechanism in dam and levee failures, accounting for nearly 50% of failures in global datasets of dams constructed from pre-1900 through the 1990s (Foster et al., 2000). Efforts to model piping initiation are therefore common in the civil engineering literature. Physical experiments and numerical models often aim to identify and predict the critical hydraulic gradients (Rice & Swainston-Fleshman, 2013; Israr & Indraratna, 2019; Alsakran et al., 2021) or critical seepage velocities (Richards & Reddy, 2012) required to initiate piping erosion in engineered and natural soils with varying textures, bulk densities, and geometric configurations. Poorly sorted soils with nonplastic fines (e.g., silt) are most susceptible and typically require the smallest hydraulic gradients—on the order of 0.2—for the onset of piping, because their particle size is fine enough to be easily detached, but they lack the plasticity and cohesion of pure clays (Rice & Swainston-Fleshman, 2013; Israr & Indraratna, 2019).

Flow through active soil pipes and the detachment and transport of sediment are more complex and less thoroughly studied (Wilson et al., 2018). Promising models that assume uniform pipe geometry and high bulk densities (Bonelli et al., 2006), conditions more typical of piping in dams and levees than on hillslopes, have limited ability to predict suspended sediment concentrations in pipeflow in studies of natural materials. In such cases, pipes are shorter, and headcutting at the open end of the pipe rapidly expands the pipe bottom near the exit (Fox et al., 2014). The variety of stresses acting on pipe margins—including shear stress from the flow, clay dispersion, and seepage forces—is difficult to describe mathematically and requires sophisticated modeling (Fox et al., 2014).

Piping has been incorporated into semi-distributed hillslope-catchment models that describe subsurface preferential flow contributions to streamflow, which have been calibrated with field data from a couple of particularly well-instrumented catchments. In the steep, humid Maimai catchment in New Zealand, Weiler and McDonnell (2004, 2007) developed a model that explicitly represents soil pipe networks. The catchment's runoff response was relatively insensitive to the exact spatial placement of pipes, provided their connectivity and activation thresholds were preserved (Weiler & McDonnell, 2004; Weiler & McDonnell, 2007). Pipes in the Maesnant catchment in Wales motivated the development of a pipeflow model in which mapped pipe density and connectivity strongly control stormflow generation (Jones & Connelly, 2002).

Both the Jones & Connelly (2002) and Weiler & McDonnell (2004, 2007) models require saturated conditions as a prerequisite for pipe flow; the phreatic surface must rise above the pipe's elevation to initiate lateral flow through the pipe. In fact, models across all scales discussed here—including local initiation, flow through active pipes, and hillslope/catchment scale—all require saturated conditions. Laboratory and field studies indicate that perched saturation along soil-rock interfaces or along textural boundaries in duplex soils contributes to pipeflow and associated subsurface erosion (Klaus & Jackson, 2018; Xu et al., 2020). The connectivity between perched layers and the water table is discontinuous and variable in both space and time (Wilson et al., 2017).

Achieving sufficient water-table rise for pipeflow, however, is not trivial. Calculations based on field infiltration rates suggest that if rainwater infiltrated only through the soil matrix, it would reach the pipes much later than the observed response time—often after peak discharge or even after the storm had ended (Jones & Connelly, 2002). This implies that crack or macropore flow dominates water delivery to the pipes, likely through indirect pathways in which cracks either capture overland flow or route infiltrating water down to the water table before it drains into the pipes (Jones & Connelly, 2002). Jones and Connelly do not directly capture this behavior in their 2002 model, noting that a combined Richards-macropore infiltration model would require calibration data beyond what is typically feasible.

1.2 Objective and hypothesis

This chapter aims to use a simple semi-analytical model to evaluate the role of soil macropores in the initiation of piping. I will use a 1D Green-Ampt infiltration model to estimate upper-bound wetting-front positions throughout an extreme precipitation event and to demonstrate whether matrix infiltration can contribute to event-timeline perched saturation under realistic conditions. By modifying the 1D Green-Ampt infiltration model to include macroporosity, I will assess the extent to which macropore flow is required to transmit water to a perched water table on timescales consistent with observed piping responses.

Hypothesis 1: Vertical macropore flow is required to produce the perched saturation that drives flow through soil pipes.

I hypothesize that matrix flow alone cannot advance modeled infiltration wetting fronts sufficiently deep within the timescales of single or compound events (1–3 days) to produce the observed piping response. Vertical macroporosity will be essential for generating the perched saturation and rapid infiltration required to trigger piping. The magnitude of this effect will depend on soil properties and the depth of the low-conductivity layer above which perched saturation develops.

2. Methodology

Prior work on piping collapse sinkholes in semiarid regions indicates that geomorphic change is more closely associated with extreme rainfall events than gradual moisture accumulation (Rafaeli et al., 2023). I therefore selected the wettest three-day period on record at the "Lamar 3" CoAgMET weather station to model the role of vertical macroporosity in generating perched saturation (Schumacher et al., 2018). The "Lamar 3" station is ~30 km northeast of SPLT and is in a similar low-relief grassland setting with comparable semi-arid hydroclimatic conditions. Field observations at SPLT similarly indicate that pipes typically flow shortly after rainfall, and only briefly (<1 day), in response to high-intensity, short-duration storms. Evidence of pipeflow included wetted channels downstream of pipe outlets (Figure 14a) and collapsed blocks of overhanging soil and vegetation (Figure 14b), and was usually accompanied by inundation of ephemeral wetlands (Figure 14c)—evidence of perched saturation.

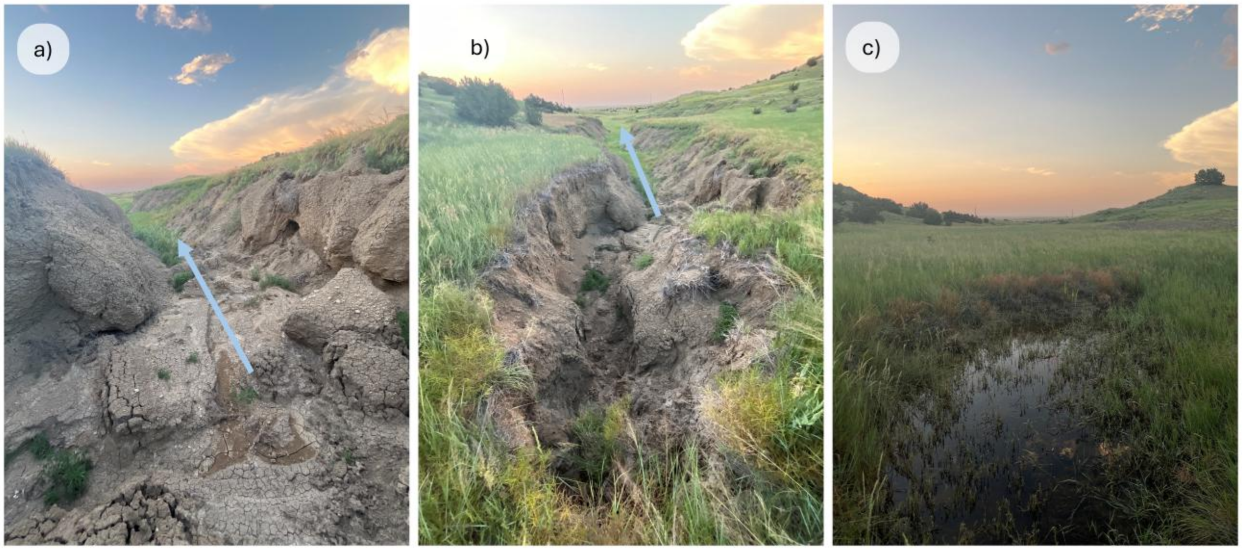

Figure 14: (a) Wetted channel (~2 m wide) downstream of piping network outlet (flow direction in blue), (b) blocks of soil and vegetation associated with piping collapse (~2 m wide), and (c) ephemeral wetland (~3 m wide) upstream of piping network.

Thus, selecting the three-day maximum precipitation represents the maximum plausible infiltration input associated with pipeflow. A three-day window was selected, somewhat arbitrarily, to capture short-term extreme rainfall accumulation and associated infiltration responses, while avoiding the underestimation that can occur with single-day totals. The three-day maximum precipitation (over the 11-year record beginning in 2014) of 11.9 cm occurred over June 6-8, 2022, and occurred in two short-duration, high-intensity bursts (Figure 15). The data had a five-minute temporal resolution; each modeled timestep was five minutes long.

I partitioned incoming rainfall (P) into matrix flow (P_m) and macropore bypass (P_b) flow (Equation 7).

$$\beta = \text{ bypass fraction } [0,1]; \quad P_m(t) = (1-\beta)P(t); \quad P_b(t) = \beta P(t) \tag{7}$$

I then routed matrix flow (P_m) downward through the soil matrix according to the Green-Ampt infiltration model (Equation 8; Green & Ampt, 1911; Brunner, 2020). The Green-Ampt model provides a physically based, semi-analytical solution for one-dimensional vertical infiltration through unsaturated porous media. The model assumes homogeneous soil properties, including hydraulic conductivity and initial water content, and prescribes a constant capillary suction head at the wetting front (Brunner, 2020). In reality, wetting fronts are gradual transitions from saturated to unsaturated conditions, but the Green-Ampt model assumes that infiltrating water pushes into the soil as a well-defined wetting front, leaving a relatively uniform wet zone above and drier soil below. The model further assumes that there is no evapotranspiration, lateral flow, or redistribution between precipitation events. As a result, Green-Ampt infiltration over the three-day wet period represents a maximum-rate approximation of wetting-front advance relative to Richards equation-based models with gradational wetting fronts, redistribution between storms, and two- or three-dimensional flow.

$$f(t) = min\,[P_m,\ K\left(1 + \frac{\psi(\theta_s - \theta_i)}{I(t)}\right)] \tag{8}$$

In Equation 8, $f(t)$ is the infiltration rate at time t. $f(t)$ is the minimum of the incoming precipitation to the soil matrix (P_m) and the infiltration capacity (the right-hand side of Equation 8). Precipitation exceeding the infiltration rate is rejected as surface runoff. K is the saturated hydraulic conductivity, averaged over the soil profile depth. I used the NRCS Web Soil Survey (Soil Survey Staff, NRCS, 2025) to extract a hydraulic conductivity of 0.24 meters per day for a silt loam mapped at SPLT in areas with piping. θ_s is the saturated water content, assumed here to be 0.45—an average value for silt loam soils as reported by Carsel and Parrish (1988). θ_i is the initial saturation prior to the three-day wet period, assumed as an upper bound value equal to field capacity, at 0.27 (Simunek et al., 2022). ψ is the wetting front suction, set here to 0.12 m—

a median value for silt loam as per the HEC-RAS Hydraulic Reference Manual (Brunner, 2020). $I(t)$ is the cumulative infiltration, summed over all preceding timesteps.

The depth of the wetting front (z) is updated at each timestep as the cumulative infiltration divided by the available saturation (Equation 9).

$$z(t) = \frac{I(t)}{\Delta\theta} \tag{9}$$

Restrictive layers (clay, shale) were observed in the field at depths of 0.75-2.5 m; the model therefore assumes a restrictive layer at the uppermost 0.75 m depth. Because the Green-Ampt model assumes homogeneous hydraulic conductivity, when the wetting front reaches this depth, vertical flow is assumed as effectively zero on event timescales (i.e., a no-flow boundary condition) due to the low hydraulic conductivity of the underlying material. At this point, any additional infiltration is assumed to contribute to lateral flow atop the layer or to surface runoff.

Apart from the wetting front reaching the low-conductivity layer, which is unlikely given observed infiltration rates (Jones & Connelly, 2002), perched water is generated primarily by macropore bypass flow. The height of the perched water table (h) is calculated as the cumulative precipitation bypassing the matrix through macropores (P_b) divided by the available saturation (Equation 10).

$$h(t) = \frac{P_{b,cum}(t)}{\Delta\theta} \tag{10}$$

I varied the macropore bypass fraction (β) from 0 to 1 in increments of 0.1 and calculated the wetting front depth and perched water table height over time. It is important to note that this fraction (β) is not the volumetric soil fraction occupied by macropores, which can be estimated in natural soils, but rather the fraction of incoming precipitation that flows rapidly through macropores. Quantifying this fraction in the field is difficult because macropore and matrix flow pathways cannot be directly observed and must instead be inferred from tracer experiments (Sheng et al., 2014).

3. Results

To evaluate the ability of matrix infiltration to reach observed restrictive layers, I first simulated the wetting front advance with $\beta = 0$ (all precipitation routed to the matrix). This scenario was used to assess whether matrix infiltration alone could supply water to depths comparable to field-observed restrictive layers (0.75-2.5 m). Figure 15a shows a hyetograph for the wettest three-day period on record. As shown in Figure 15b, the modeled infiltration wetting front associated with this wet period only reaches ~0.4 m within the three-day modeled period. Even if all of the precipitation is directed to the soil matrix ($\beta = 0$), vertical matrix flow cannot produce the perched saturated conditions requisite for soil piping in semiarid grasslands.

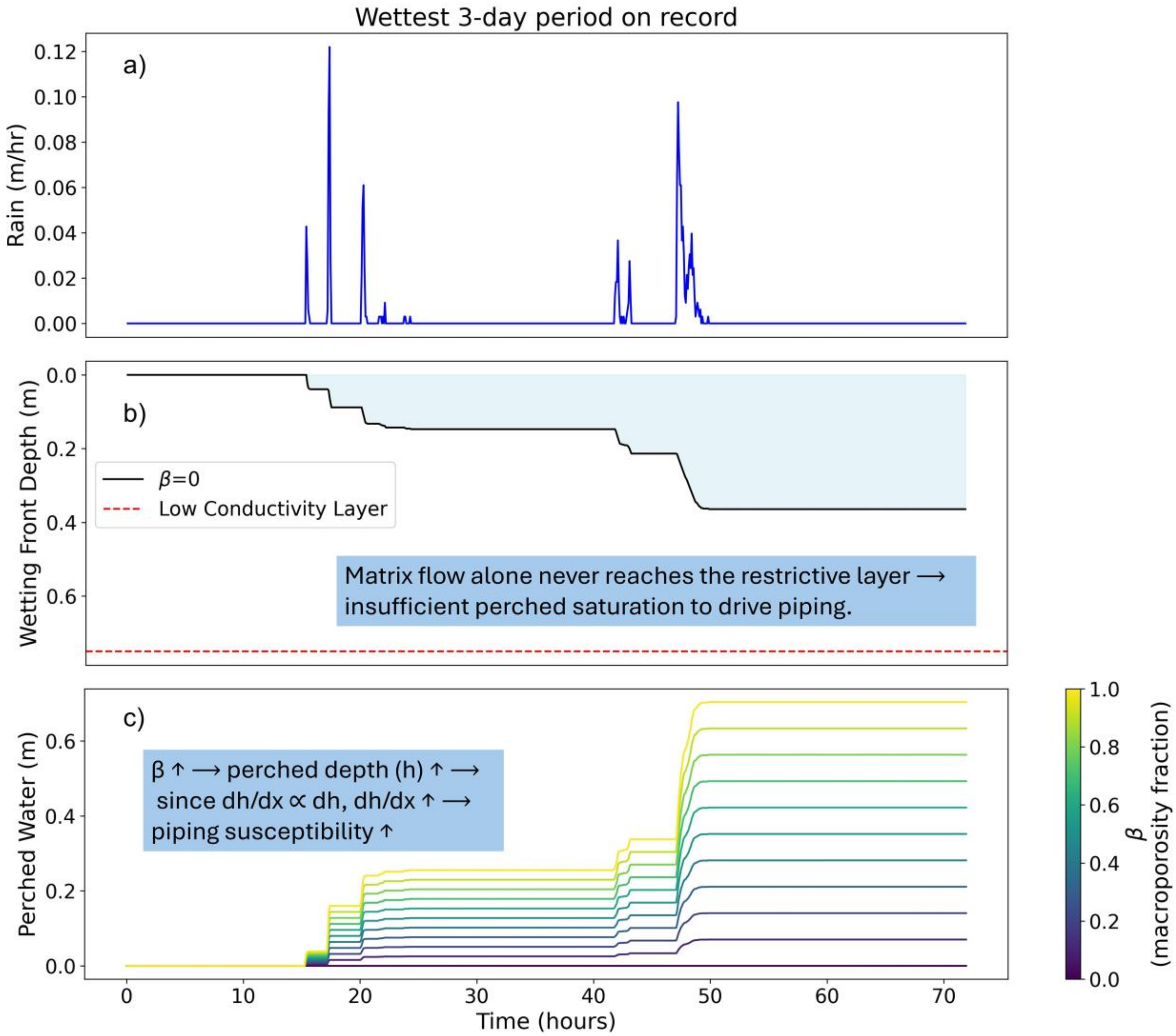

Figure 15: (a) Hyetograph for the wettest three-day period on record near SPLT, (b) modeled wetting front depth, and (c) perched water depth.

Figure 15c shows that the height (h) of the perched water table increases as the fraction (β) of incoming precipitation bypassing the soil matrix through vertical macropores increases. Only when rapid, deep infiltration ($\beta > 0$) is present does perched saturation develop, leading to increases in perched depth capable of increasing the hydraulic gradient and piping susceptibility. In reality, lateral flow and redistribution between events would likely decrease the height of the perched water table.

The modeled response demonstrates that, in general, flow through vertical macropores likely dominates the transmission of rainwater to pipes. I did not collect sufficient subsurface data to constrain pipe length or the location of perched layers and thus could not compute the hydraulic gradient. Since the lateral hydraulic gradient (dh/dx) scales with the change in hydraulic head (dh), we can infer that greater water infiltration through vertical macroporosity networks, which increases perched water (i.e., an increase in h; Figure 15c), locally steepens lateral hydraulic gradients. This increase in hydraulic gradient may be sufficient to cross critical thresholds and initiate piping, depending on the soil texture and dispersive properties (Israr & Indraratna, 2019). Perched saturation and the hydraulic gradient are also influenced by topographic and geologic controls, including the slope, the bedrock dip angle, and flow through rock fractures.

4. Discussion

Changes in macroporosity modulate the transmission of water to pipes. Even during the wettest three-day period on record and with the optimistic assumptions of the Green-Ampt infiltration model, the soil matrix wetting front did not reach the restrictive layer or generate perched saturation within the expected three-day timeframe for pipeflow. Jones and Connelly (2002) note that matrix infiltration measured in the field with a Guelph permeameter and a double-ring infiltrometer similarly yielded vertical infiltration rates too slow to supply piping networks. This suggests that matrix infiltration capacity is insufficient to explain pipe initiation; instead, pipe initiation depends on the presence of vertical preferential flow pathways that bypass the soil matrix and transmit water to depth.

In semiarid grassland systems, vertical macropores include, but are not limited to, root channels, desiccation cracks, and animal burrows (e.g., prairie dog and tarantula burrows).

Changes in burrowing animal populations in response to land management may thus influence soil piping. Grazing soils with shrink-swell clays increases desiccation cracking (Reid & Parkinson, 1984) which, in turn, increases the delivery of water to piping networks. The decay of root canals following consumptive grazing may likewise create macropores that rapidly supply perched water tables and form piping networks (Qu et al., 2025). Further, grazing-induced compaction (Chapter 2) and post-grazing decompaction reflect the collapse and redevelopment of small macropores formed around aggregates or due to bioturbation, which could also impact rapid infiltration. A study of pipe networks in Belgium found that 97% of the piping sites investigated were areas of grazed pasture (Verachtert et al., 2010). Given the extensive land-use history and the ubiquity of grazing in Northern Europe and North America's grasslands, it is not possible to directly attribute piping to grazing. It is nevertheless plausible that grazing could affect the natural processes driving piping initiation by altering surface macroporosity.

Figure 16 presents a conceptual model of the drivers of soil piping in semiarid grassland systems. Short blue arrows indicate slow matrix infiltration, whereas long blue arrows indicate rapid macropore infiltration. Infiltrating water reaches a restrictive layer, where perched saturation occurs, driving lateral flow (q_x). Eventually, this lateral flow exceeds a critical hydraulic gradient, causing erosion of subsurface pipes. Figure 16 also depicts an amphitheater-shaped piping collapse hole and the surface discharge (Q) that emerges through pipes from the collapse face. The specific contributors to vertical macroporosity shown in Figure 16 reflect conditions at SPLT and may differ across other grassland systems.

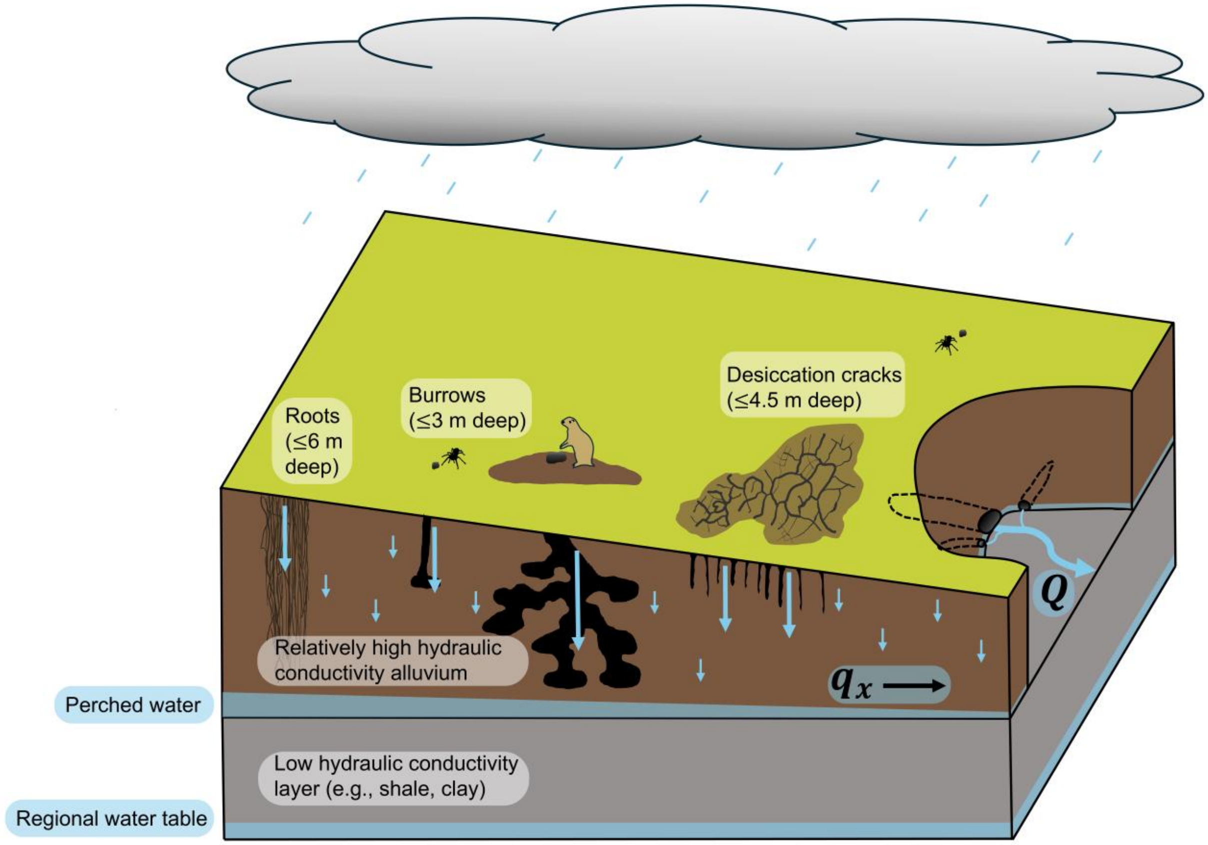

Figure 16: A conceptual model, depicting the drivers of subsurface soil pipe initiation in semiarid grasslands.

Jones and Connelly (2002) note that calibrating a coupled Richards-macropore model may require more data than is practically attainable. Since the 2002 publication of Jones and Connelly's model, significant advances (e.g., Hydrus 1D Version 4.0, first released in 2008) in variably saturated flow modeling have improved dual-permeability Richards-based models that can incorporate both matrix and macropore flow (Šimůnek et al., 2022). To develop such models, matrix properties can be reasonably estimated from literature values, as they are well-studied and readily available in published reference tables and modeling software environments (e.g., Carsel & Parrish, 1988; Šimůnek et al., 2022). Significant uncertainty remains in quantifying the spatial extent, hydraulic properties, and connectivity of macropores, suggesting that future work should focus on constraining macropore properties. The model presented here does not explicitly simulate flow within vertical macropores but rather demonstrates that such pathways are required to explain the observed behavior. If field-derived macropore properties can be estimated, a dual-permeability infiltration model with macropore flow could be integrated into existing frameworks (e.g., Jones & Connelly, 2002; Weiler & McDonnell, 2004, 2007) to improve understanding of catchment responses to piping from the onset of precipitation.

Given the extreme nature of rainfall events that supply pipe networks, it is also important to consider the compound influence that overland flow exerts on piping collapse holes and headcuts. Overland flow has been well documented in settings similar to SPLT in southeastern Colorado (Rengers & Tucker, 2015), and some areas underlain by piping networks at SPLT also exhibit a consistent downslope orientation of flattened grass, indicating overland flow. Overland flow concentrates at headcut apices and promotes deeper infiltration and saturation there, increasing the likelihood of mass failure and contributing to the continued headward erosion of piping collapse features (Rengers & Tucker, 2015). Plunge pool erosion over the headcut lip moves already-collapsed material and creates ponded water and saturated conditions at the base of the headcut wall, further contributing to mass failure (Rengers & Tucker, 2015). Desiccation cracks and other vertical macropores may also capture overland flow, transmitting more water to piping networks than precipitation alone could account for (Jones & Connelly, 2002).

5. Conclusions

In this chapter, I used a simple one-dimensional Green-Ampt vertical infiltration model to demonstrate that soil matrix infiltration is too slow to deliver water to perched saturated layers and initiate the erosion of soil piping networks. Rapid infiltration through vertical macropores is therefore requisite for piping in semiarid grasslands. Soil piping is a natural consequence of subsurface flow in media with vertical heterogeneity in hydraulic conductivity, but alterations in vertical macroporosity are likely to affect a soil's susceptibility to subsurface pipe erosion. Concerned land managers and restoration practitioners should therefore aim to understand whether and how historic land use has impacted vertical macroporosity (e.g., whether the death of perennial grasses has promoted root-cavity macropores and desiccation cracking), and implement landscape-scale management practices to address these problems.

References

Alsakran, M. A., Zhu, J. G., & Er-Lu, W. (2021). Experimental study for assessing the onset of suffusion and suffosion of gap-graded soil. *Soil Mechanics and Foundation Engineering*, *57*(6), 458-464.

Bernatek-Jakiel, A., & Nadal-Romero, E. (2023). Can soil piping impact environment and society? Identifying new research gaps. *Earth Surface Processes and Landforms*, *48*(1), 72-86.

Bonelli, S., Brivois, O., Borghi, R., & Benahmed, N. (2006). On the modelling of piping erosion. *Comptes Rendus Mécanique*, *334*(8-9), 555-559.

Brunner, G. W. (2020). HEC-RAS river analysis system. Hydraulic reference manual. Version 6.0.

Bryan, R. B & Jones, J. A. (1997). The significance of soil piping processes: inventory and prospect. *Geomorphology*, *20*, 209-218.

Carsel, R. F., & Parrish, R. S. (1988). Developing joint probability distributions of soil water retention characteristics. *Water resources research*, *24*(5), 755-769.

Foster, M., Fell, R., & Spannagle, M. (2000). The statistics of embankment dam failures and accidents. *Canadian Geotechnical Journal*, *37*(5), 1000-1024.

Fox, G. A., Felice, R. G., Midgley, T. L., Wilson, G. V., & Al-Madhhachi, A. S. T. (2014). Laboratory soil piping and internal erosion experiments: evaluation of a soil piping model for low-compacted soils. *Earth Surface Processes and Landforms*, *39*(9), 1137-1145.

Green, W.H., and Ampt, G.A. 1911. Studies on soil physics, *Journal of Agricultural Science*, 4(1), 1–24.

Israr, J., & Indraratna, B. (2019). Study of critical hydraulic gradients for seepage-induced failures in granular soils. *Journal of Geotechnical and Geoenvironmental Engineering*, *145*(7), 04019025.

Jones, J. A. A. (2010). Soil piping and catchment response. *Hydrological Processes*, *24*(12), 1548-1566.

Jones, J. A. A., & Connelly, L. J. (2002). A semi-distributed simulation model for natural pipeflow. *Journal of Hydrology*, *262*(1-4), 28-49.

Klaus, J., & Jackson, C. R. (2018). Interflow is not binary: A continuous shallow perched layer does not imply continuous connectivity. *Water Resources Research*, *54*(9), 5921-5932.

Rafaeli, O., Nahlieli, A., & Svoray, T. (2023). Dynamics of subsurface soil erosion in a semiarid region: A time-series study of sinkhole area and morphology. *Catena*, *233*, 107511.

Reid, I., & Parkinson, R. J. (1984). The wetting and drying of a grazed and ungrazed clay soil. *Journal of Soil Science*, *35*(4), 607–614.

Rengers, F. K., & Tucker, G. E. (2015). The evolution of gully headcut morphology: a case study using terrestrial laser scanning and hydrological monitoring. *Earth Surface Processes and Landforms*, *40*(10), 1304-1317.

Rice, J., & Swainston-Fleshman, M. (2013). Laboratory modeling of critical hydraulic conditions for the initiation of piping. In *Geo-Congress 2013: Stability and Performance of Slopes and Embankments III* (pp. 1044-1055).

Richards, K. S., & Reddy, K. R. (2012). Experimental investigation of initiation of backward erosion piping in soils. *Géotechnique*, *62*(10), 933-942.

Schumacher, R. S., Goble, P. E., Schwalbe, Z., & Bolinger, R. A. (2018). Using CoAgMET, "Colorado's Mesonet," to analyze our state's weather and climate. *Colorado Water, 35*(5).

Sheng, F., Liu, H., Wang, K., Zhang, R., & Tang, Z. (2014). Investigation into preferential flow in natural unsaturated soils with field multiple-tracer infiltration experiments and the active region model. *Journal of hydrology*, *508*, 137-146.

Šimůnek J, Šejna M, Brunetti G, van Genuchten M. Th. (2022). The HYDRUS Software Package for Simulating the One-, Two-, and Three-Dimensional Movement of Water, Heat, and Multiple Solutes in Variably Saturated Media, Technical Manual I, Hydrus 1D, Version 5.0. PC Progress, Prague, Czech Republic; 334.

Swanson, M. L., Kondolf, G. M., & Boison, P. J. (1989). An example of rapid gully initiation and extension by subsurface erosion: coastal San Mateo County, California. *Geomorphology*, *2*(4), 393-403.

Verachtert, E., Van Den Eeckhaut, M., Poesen, J., & Deckers, J. (2010). Factors controlling the spatial distribution of soil piping erosion on loess-derived soils: A case study from central Belgium. *Geomorphology*, *118*(3-4), 339-348.

Weiler, M., & McDonnell, J. (2004). Virtual experiments: a new approach for improving process conceptualization in hillslope hydrology. *Journal of Hydrology*, *285*(1-4), 3-18.

Weiler, M., & McDonnell, J. J. (2007). Conceptualizing lateral preferential flow and flow networks and simulating the effects on gauged and ungauged hillslopes. *Water Resources Research*, *43*(3).

Wilson, G. V., Nieber, J. L., Fox, G. A., Dabney, S. M., Ursic, M., & Rigby, J. R. (2017). Hydrologic connectivity and threshold behavior of hillslopes with fragipans and soil pipe networks. *Hydrological Processes*, *31*(13), 2477-2496.

Wilson, G. V., Wells, R., Kuhnle, R., Fox, G., & Nieber, J. (2018). Sediment detachment and transport processes associated with internal erosion of soil pipes. *Earth Surface Processes and Landforms*, *43*(1), 45-63.

Xu, X., Wilson, G. V., Zheng, F., & Tang, Q. (2020). The role of soil pipe and pipeflow in headcut migration processes in loessic soils. *Earth Surface Processes and Landforms*, *45*(8), 1749-1763.

CHAPTER 4: SYNTHESIS AND FUTURE DIRECTIONS

In the first chapter of this thesis, I evaluated post-grazing recovery and structural restoration outcomes in semiarid grasslands. Grazing-induced compaction recovered after roughly a decade, whereas remotely sensed upland vegetation did not recover on a landscape scale within the observation window. Future investigations of grassland recovery and restoration could incorporate quadrat-based field monitoring of upland vegetation. Time and budget constraints prevented me from doing so in this project, but such data would enable the development of ground-truth training and testing datasets for remote sensing-based machine learning models capable of predicting the actual percentage of bare soil across the landscape. This would go beyond the index-based approach used here, which is physically grounded but yields relative, unitless measures that cannot be directly converted into quantitative estimates of ground cover. This could be especially useful in understanding the long-term recovery trajectory and the impacts of bison as SPLT's herd continues to interact with the landscape. Further, because purely satellite-based monitoring methods may be ineffective at detecting patch-, plant-, and subsurface-scale vegetation recovery, quadrat-based monitoring may help constrain these important aspects of vegetation response.

In small catchments where erosion is dominated by piping collapse, structures generally remained intact but had little geomorphic effect because there was limited surface flow to transport sediment. In large catchments, erosion was driven by both subsurface and surface processes; flash floods in such areas destroyed many structures, but intact structures often captured sediment, especially in steep, bare, recently grazed sites. I grouped restoration structures placed in similar geomorphic contexts, evaluating the collective outcome of each cluster rather than the interactions among individual structures. Future work could explicitly examine the geomorphic and hydrologic effects of multiple structures in sequence to better understand how their proximity to one another influences performance.

Whether evaluated individually or in clusters, erosion control structures were unlikely to have any geomorphic effect in small catchments where erosion is dominated by the collapse of subsurface soil piping networks. This observation motivated the second chapter of this thesis, in which I used numerical methods to examine how land management actions may affect piping susceptibility. I found that vertical flow through soil macropores, rather than flow through the soil matrix, governs water delivery to perched saturated layers and the initiation of soil piping. Future studies investigating conditions and management practices that influence macroporosity could inform catchment-scale hydrologic models that explicitly incorporate piping networks. Specifically, field investigations quantifying the spatial extent (surface and subsurface) and connectivity, as well as the hydraulic properties, of desiccation cracks, root cavities, and animal burrows could inform models that account for macropore contributions to pipe initiation and flow.

Further, applying modern techniques such as optically stimulated luminescence and carbon dating could help date alluvial surfaces, constrain erosion rates, and develop a more complete understanding of both soil piping processes and broader landscape evolution in semiarid grassland systems.

APPENDIX 1—DATA

Table 5: Soil bulk density data for each parcel and soil texture class.

Parcel	Texture Class	Sample	Mass (g)	Bulk Density (g/mL)	Latitude	Longitude
B	2	1	126	1.16	37.74711	-102.94750
B	2	2	116	1.07	37.74788	-102.94727
B	2	3	115	1.06	37.74975	-102.94734
B	2	4	131	1.21	37.75071	-102.93650
B	2	5	145	1.34	37.75135	-102.94563
B	2	6	104	0.96	37.75198	-102.94466
B	2	7	138	1.27	37.75249	-102.94377
B	2	8	101	0.93	37.75333	-102.94300
B	2	9	96	0.89	37.75416	-102.94228
B	2	10	116	1.07	37.7545	-102.94144
B	3	1	100	0.92	37.73139	-102.93558
B	3	2	111	1.02	37.73148	-102.93559
B	3	3	110	1.01	37.73161	-102.93572
B	3	4	76	0.70	37.73167	-102.92592
B	3	5	96	0.89	37.73181	-102.93592
B	3	6	90	0.83	37.73202	-102.93597
B	3	7	99	0.91	37.7322	-102.93591
B	3	8	106	0.98	37.7324	-102.93602
B	3	9	93	0.86	37.73256	-102.93606
B	3	10	101	0.93	37.73283	-102.93614
B	4	1	109	1.01	37.73148	-102.92437
B	4	2	104	0.96	37.73182	-102.92435
B	4	3	109	1.01	37.73239	-102.92447
B	4	4	114	1.05	37.73309	-102.92467
B	4	5	95	0.88	37.73332	-102.92522
B	4	6	94	0.87	37.73343	-102.92585
B	4	7	105	0.97	37.73367	-102.92661
B	4	8	122	1.13	37.73324	-102.92697
B	4	9	121	1.12	37.73284	-102.92660
B	4	10	114	1.05	37.73198	-102.92579
B	5	1	86	0.79	37.73146	-102.93902
B	5	2	100	0.92	37.73205	-102.93913
B	5	3	111	1.02	37.73283	-102.93929
B	5	4	96	0.89	37.73331	-102.93970
B	5	5	84	0.77	37.73354	-102.94032
B	5	6	96	0.89	37.73362	-102.94121

B	5	7	102	0.94	37.73347	-102.94182
B	5	8	104	0.96	37.73298	-102.94167
B	5	9	95	0.88	37.73233	-102.94145
B	5	10	114	1.05	37.73172	-102.94076
A	2	1	109	1.01	37.76163	-102.88462
A	2	2	113	1.04	37.76138	-102.88432
A	2	3	101	0.93	37.76108	-102.88409
A	2	4	117	1.08	37.76081	-102.88397
A	2	5	101	0.93	37.76054	-102.88409
A	2	6	121	1.12	37.7607	-102.88386
A	2	7	105	0.97	37.76094	-102.88344
A	2	8				
A	2	9	105	0.97	37.76086	-102.883
A	2	10	100	0.92	37.76111	-102.8828
A	3	1	130	1.20	37.73755	-102.8934
A	3	2	85	0.78	37.73767	-102.8932
A	3	3	94	0.87	37.73775	-102.8929
A	3	4	118	1.09	37.73806	-102.8926
A	3	5	116	1.07	37.73838	-102.8926
A	3	6	118	1.09	37.73876	-102.8926
A	3	7	111	1.02	37.73903	-102.8928
A	3	8	103	0.95	37.73937	-102.893
A	3	9	124	1.14	37.73981	-102.8929
A	3	10				
A	4	1	104	0.96	37.76148	-102.8936
A	4	2	117	1.08	37.76102	-102.893
A	4	3	116	1.07	37.76076	-102.8928
A	4	4	111	1.02	37.76055	-102.8927
A	4	5	113	1.04	37.7603	-102.8925
A	4	6	109	1.01	37.76006	-102.8923
A	4	7	105	0.97	37.75983	-102.8925
A	4	8	115	1.06	37.75985	-102.8928
A	4	9	115	1.06	37.7601	-102.8931
A	4	10	97	0.89	37.76048	-102.8934
A	5	1	111	1.02	37.76744	-102.8935
A	5	2	103	0.95	37.76732	-102.8933
A	5	3	119	1.10	37.76724	-102.893
A	5	4	90	0.83	37.76716	-102.8927
A	5	5	108	1.00	37.76709	-102.8924
A	5	6	102	0.94	37.76702	-102.8921

A	5	7	118	1.09	37.76698	-102.8919
A	5	8	105	0.97	37.76694	-102.8916
A	5	9	120	1.11	37.7669	-102.8913
A	5	10	121	1.12	37.76689	-102.891
F	2	1	150	1.38	37.78992	-102.8711
F	2	2	155	1.43	37.7902	-102.871
F	2	3	134	1.24	37.79042	-102.871
F	2	4	107	0.99	37.79155	-102.8698
F	2	5	125	1.15	37.79169	-102.8697
F	2	6	152	1.40	37.79141	-102.87
F	2	7	145	1.34	37.79126	-102.8702
F	2	8	132	1.22	37.79105	-102.8703
F	2	9	112	1.03	37.79085	-102.8705
F	2	10	138	1.27	37.79063	-102.8707
F	3	1	155	1.43	37.79862	-102.8557
F	3	2	148	1.37	37.79884	-102.8556
F	3	3	145	1.34	37.79909	-102.8554
F	3	4	128	1.18	37.79928	-102.8553
F	3	5	155	1.43	37.79945	-102.855
F	3	6	157	1.45	37.79963	-102.8551
F	3	7	150	1.38	37.79981	-102.855
F	3	8	148	1.37	37.79996	-102.8549
F	3	9	139	1.28	37.80013	-102.8548
F	3	10	140	1.29	37.80031	-102.8547
F	4	1	141	1.30	37.79044	-102.8661
F	4	2	136	1.25	37.79012	-102.8665
F	4	3	150	1.38	37.79068	-102.8659
F	4	4	136	1.25	37.79093	-102.8659
F	4	5	151	1.39	37.79119	-102.8659
F	4	6	135	1.25	37.79148	-102.8661
F	4	7	116	1.07	37.79176	-102.8661
F	4	8	123	1.13	37.79192	-102.866
F	4	9	129	1.19	37.7921	-102.8656
F	4	10	125	1.15	37.79238	-102.865
F	5	1	113	1.04	37.82371	-102.8192
F	5	2	131	1.21	37.82396	-102.8193
F	5	3	131	1.21	37.8242	-102.8194
F	5	4	127	1.17	37.82441	-102.8194
F	5	5	118	1.09	37.82454	-102.8195
F	5	6	120	1.11	37.82484	-102.8196

F	5	7	124	1.14	37.82583	-102.82
F	5	8	146	1.35	37.82512	-102.8197
F	5	9	131	1.21	37.82534	-102.8198
F	5	10	99	0.91	37.82553	-110.1928
D	2	1	135	1.25	37.79044	-102.8616
D	2	2	127	1.17	37.79019	-102.8613
D	2	3	148	1.37	37.79013	-102.8611
D	2	4	136	1.25	37.78996	-102.861
D	2	5	138	1.27	37.78963	-102.8609
D	2	6	169	1.56	44.89361	-102.861
D	2	7	151	1.39	37.789	-102.8613
D	2	8	159	1.47	37.78885	-102.8614
D	2	9	147	1.36	37.78869	-102.8616
D	2	10	134	1.24	37.78846	-102.8616
D	3	1	118	1.09	37.80126	-102.8937
D	3	2	109	1.01	37.80143	-102.8934
D	3	3	123	1.13	37.80146	-102.8931
D	3	4	117	1.08	37.80164	-102.8929
D	3	5	112	1.03	37.80188	-102.8926
D	3	6	120	1.11	37.80214	-102.8926
D	3	7	113	1.04	37.80226	-102.8924
D	3	8	122	1.13	37.80252	-102.8924
D	3	9	131	1.21	37.80276	-102.8926
D	3	10	130	1.20	37.80302	-102.8922
D	4	1	115	1.06	37.78926	-102.8659
D	4	2	114	1.05	37.78927	-102.8657
D	4	3	132	1.22	37.78901	-102.8656
D	4	4	122	1.13	37.78886	-102.8664
D	4	5	125	1.15	37.78864	-102.8667
D	4	6	130	1.20	37.78831	-102.8667
D	4	7	125	1.15	37.78793	-102.8668
D	4	8	111	1.02	37.78777	-102.8667
D	4	9	112	1.03	37.78757	-102.8666
D	4	10	111	1.02	37.78725	-102.8666
D	5	1	138	1.27	37.76773	-102.8935
D	5	2	132	1.22	37.76796	-102.8934
D	5	3	135	1.25	37.76825	-102.8932
D	5	4	135	1.25	37.7685	-102.893
D	5	5	122	1.13	37.76872	-102.8929
D	5	6	105	0.97	37.76898	-102.8927

D	5	7	135	1.25	37.76918	-102.8925
D	5	8	128	1.18	37.7694	-102.8923
D	5	9	116	1.07	37.76962	-102.8921
D	5	10	118	1.09	37.76974	-102.892
E	2	1	143	1.32	37.79429	-102.8188
E	2	2	121	1.12	37.79408	-102.8187
E	2	3	115	1.06	37.79372	-102.8186
E	2	4	127	1.17	37.79352	-102.8186
E	2	5	118	1.09	37.7933	-102.8185
E	2	6	133	1.23	37.793	-102.8184
E	2	7	133	1.23	37.79278	-102.8182
E	2	8	115	1.06	37.79252	-102.8184
E	2	9	125	1.15	37.79242	-102.8187
E	2	10	123	1.13	37.79242	-102.8189
E	3	1	101	0.93	37.80321	-102.8019
E	3	2	129	1.19	37.80303	-102.8016
E	3	3	121	1.12	37.80287	-102.8013
E	3	4	124	1.14	37.8027	-102.801
E	3	5	116	1.07	37.80254	-102.8006
E	3	6	109	1.01	37.80237	-102.8004
E	3	7	126	1.16	37.80222	-102.8001
E	3	8	111	1.02	37.80199	-102.8
E	3	9	142	1.31	37.80178	-102.7997
E	3	10	136	1.25	37.80194	-102.7993
E	4	1	130	1.20	37.8012	-102.8198
E	4	2	133	1.23	37.80096	-102.8198
E	4	3	133	1.23	37.80089	-102.8199
E	4	4	118	1.09	37.80048	-102.8198
E	4	5	122	1.13	37.80017	-102.82
E	4	6	129	1.19	37.79999	-102.8201
E	4	7	137	1.26	37.79977	-102.8201
E	4	8	152	1.40	37.79971	-102.8201
E	4	9	115	1.06	37.7994	-102.8202
E	4	10	119	1.10	37.7992	-102.8202
E	5	1	131	1.21	37.80326	-102.7915
E	5	2	134	1.24	37.8037	-102.7916
E	5	3	133	1.23	37.80379	-102.7915
E	5	4	122	1.13	37.80408	-102.7915
E	5	5	126	1.16	37.80451	-102.7914
E	5	6	130	1.20	37.80457	-102.7913

E	5	7	113	1.04	37.80476	-102.7912
E	5	8	124	1.14	37.80506	-102.791
E	5	9	99	0.91	37.80538	-102.7909
E	5	10	117	1.08	37.80558	-102.7908
C	2	1	117	1.08	37.78148	-102.9662
C	2	2	130	1.20	37.78141	-102.966
C	2	3	124	1.14	37.70135	-102.9657
C	2	4	148	1.37	37.78116	-102.9654
C	2	5	140	1.29	37.78111	-102.9652
C	2	6	124	1.14	37.78104	-102.9648
C	2	7	133	1.23	37.78104	-102.9645
C	2	8	140	1.29	37.78094	-102.9643
C	2	9	140	1.29	37.78074	-102.964
C	2	10	125	1.15	37.78079	-102.9637
C	3	1	164	1.51	37.79582	-102.9639
C	3	2	130	1.20	37.79602	-102.9638
C	3	3	129	1.19	37.79627	-102.9637
C	3	4	132	1.22	37.79643	-102.9635
C	3	5	129	1.19	37.7966	-102.9635
C	3	6	126	1.16	37.79678	-102.9634
C	3	7	131	1.21	37.79693	-102.9633
C	3	8	125	1.15	37.79733	-102.9634
C	3	9	124	1.14	37.79757	-102.9636
C	3	10	127	1.17	37.79771	-102.9639
C	4	1	138	1.27	37.76291	-102.9663
C	4	2	118	1.09	37.76277	-102.866
C	4	3	133	1.23	37.7627	-102.9688
C	4	4	113	1.04	37.76255	-102.9656
C	4	5	128	1.18	37.76241	-102.9655
C	4	6	124	1.14	37.76237	-102.9654
C	4	7	128	1.18	37.76223	-102.9651
C	4	8	104	0.96	37.76217	-102.9649
C	4	9	116	1.07	37.76197	-102.9646
C	4	10	114	1.05	37.76181	-102.9643
C	5	1	117	1.08	37.76972	-102.9663
C	5	2	122	1.13	37.76976	-102.9661
C	5	3	125	1.15	37.76986	-102.9658
C	5	4	119	1.10	37.77001	-102.9655
C	5	5	117	1.08	37.77005	-102.9652
C	5	6	110	1.01	37.77016	-102.9649

C	5	7	130	1.20	37.77026	-102.9647
C	5	8	127	1.17	37.77037	-102.9644
C	5	9	125	1.15	37.77049	-102.9642
C	5	10	121	1.12	37.77062	-102.964

Table 6: Remotely sensed median growing season (May-Sept.) bare soil index (BSI) values for each parcel by year.

Parcel	Year	Median BSI	Grazing	Growing Season Precipitation (mm)
E	2024	0.166787	Recent	241.3
C	2024	0.190137	Recent	241.3
F	2024	0.195089	Recent	241.3
A	2024	0.182804	Historic	241.3
B	2024	0.184045	Historic	241.3
D	2024	0.192817	Recent	241.3
E	2023	0.094184	Recent	353.314
C	2023	0.107319	Recent	353.314
F	2023	0.123044	Recent	353.314
A	2023	0.083907	Historic	353.314
B	2023	0.085744	Historic	353.314
D	2023	0.115038	Recent	353.314
E	2022	0.114006	Recent	329.438
C	2022	0.154298	Recent	329.438
F	2022	0.14069	Recent	329.438
A	2022	0.156626	Historic	329.438
B	2022	0.167694	Historic	329.438
D	2022	0.151534	Recent	329.438
E	2021	0.14356	Recent	326.136
C	2021	0.175761	Recent	326.136
F	2021	0.144472	Recent	326.136
A	2021	0.157281	Historic	326.136
B	2021	0.164563	Historic	326.136
D	2021	0.170621	Recent	326.136
E	2020	0.174835	Recent	169.418
C	2020	0.189068	Recent	169.418
F	2020	0.191451	Recent	169.418
A	2020	0.186981	Historic	169.418
B	2020	0.184048	Historic	169.418
D	2020	0.193153	Recent	169.418

E	2019	0.132096	Recent	196.342
C	2019	0.16193	Recent	196.342
F	2019	0.176549	Recent	196.342
A	2019	0.129612	Historic	196.342
B	2019	0.134198	Historic	196.342
D	2019	0.16038	Recent	196.342
E	2018	0.170152	Recent	187.452
C	2018	0.147378	Recent	187.452
F	2018	0.171895	Recent	187.452
A	2018	0.15424	Historic	187.452
B	2018	0.150129	Historic	187.452
D	2018	0.158403	Recent	187.452
E	2017	0.111699	Recent	304.8
C	2017	0.114438	Recent	304.8
F	2017	0.121519	Recent	304.8
A	2017	0.109168	Historic	304.8
B	2017	0.104734	Historic	304.8
D	2017	0.115047	Recent	304.8
E	2016	0.147612	Recent	176.53
C	2016	0.167372	Recent	176.53
F	2016	0.180921	Recent	176.53
A	2016	0.154012	Historic	176.53
B	2016	0.154038	Historic	176.53
D	2016	0.161442	Recent	176.53
E	2015	0.154734	Recent	331.724
C	2015	0.148093	Recent	331.724
F	2015	0.148315	Recent	331.724
A	2015	0.150741	Historic	331.724
B	2015	0.145357	Historic	331.724
D	2015	0.1631	Recent	331.724
E	2014	0.144746	Recent	223.012
C	2014	0.146391	Recent	223.012
F	2014	0.162602	Recent	223.012
A	2014	0.142219	Historic	223.012
B	2014	0.148081	Historic	223.012
D	2014	0.155334	Recent	223.012

Table 7: In-channel restoration structure data.

Preserve	Type	Year	Geomorph Change	Intact	Bank angle (°)	Bank veg	Headcut	DA (sqkm)	K factor	Local Slope	Grazing	Longitude	Latitude
Heartland	PALS	2021	N	Y	45.6	sparse	N	1.023	0.24	0.0117	Historic	-102.904	37.68525
Heartland	PALS	2021	N	Y	61.1	sparse	N	1.026	0.24	0.0174	Historic	-102.904	37.6853
Heartland	PALS	2021	N	Y	69.3	heavy	N	1.052	0.24	2.59E-05	Historic	-102.905	37.68608
Heartland	PALS	2021	N	Y	81.5	sparse	N	1.065	0.24	1.86E-05	Historic	-102.905	37.68627
Heartland	PALS	2021	N	Y	37.8	sparse	N	0.116	0.49	0.0433	Historic	-102.902	37.68732
Heartland	PALS	2021	N	Y	26.7	sparse	N	0.116	0.49	0.0425	Historic	-102.902	37.68731
Heartland	PALS	2021	N	Y	64.1	sparse	N	0.116	0.49	0.0427	Historic	-102.902	37.68731
Heartland	ORD	2021	N	Y	31.4	sparse	N	0.005	0.32	0.0466	Historic	-102.897	37.68778
Heartland	ORD	2021	N	Y	10.5	sparse	N	0.005	0.32	0.0470	Historic	-102.897	37.68778
Heartland	ORD	2021	N	Y	50.7	sparse	Y	0.006	0.49	0.0355	Historic	-102.897	37.68795
Heartland	ORD	2021	Y	Y	13.0	heavy	N	0.005	0.32	0.206	Historic	-102.894	37.68723
Heartland	ORD	2021	Y	Y	51.1	sparse	N	0.005	0.32	0.0826	Historic	-102.894	37.68727
Heartland	ORD	2021	Y	Y	61.5	bare	Y	0.042	0.32	0.0475	Historic	-102.894	37.68699
Heartland	Zuni	2021	Y	Y	16.8	heavy	N	0.022	0.32	0.0706	Historic	-102.894	37.68806
Heartland	ORD	2021	N	Y	8.7	heavy	Y	0.073	0.24	0.0660	Historic	-102.894	37.68815
Heartland	ORD	2023	Y	Y	16.7	bare	N	0.076	0.24	0.0475	Historic	-102.893	37.68851
Heartland	ORD	2023	Y	Y	20.7	heavy	N	0.085	0.24	0.0608	Historic	-102.893	37.68878
Heartland	ORD	2023	Y	Y	29.1	sparse	N	0.091	0.24	0.0425	Historic	-102.893	37.68917
Heartland	PALS	2023	N	Y	67.5	bare	Y	1.034	0.24	0.0384	Historic	-102.893	37.69
Heartland	PALS	2023	N	Y	68.7	heavy	N	1.061	0.24	1.56E-05	Historic	-102.893	37.69029
Heartland	ORD	2023	N	Y	42.8	heavy	Y	4.888	0.49	0.0152	Recent	-102.868	37.79037
Heartland	PALS	2024	Y	Y	49.5	sparse	N	5.015	0.32	0.00726	Recent	-102.867	37.79162
Heartland	PALS	2024	Y	Y	85.3	heavy	N	5.370	0.32	0.0655	Recent	-102.865	37.79228
Heartland	ORD	2024	Y	Y	38.7	sparse	N	5.349	0.32	0.0214	Recent	-102.865	37.79225
Heartland	ORD	2024	Y	Y	27.7	bare	N	5.304	0.32	1.23E-05	Recent	-102.864	37.79192
Heartland	ORD	2024	Y	Y	28.8	sparse	N	5.090	0.43	1.72E-05	Recent	-102.862	37.79073

Raven's	ORD	2022	N	Y	14.5	heavy	N	8.910	0.49	0.0136	Historic	-103.125	37.86814
Raven's	ORD	2022	N	Y	27.2	heavy	N	9.141	0.49	0.00871	Historic	-103.126	37.86802
Raven's	Zuni	2022	N	Y	27.4	heavy	Y	9.157	0.49	0.0120	Historic	-103.127	37.86781
Raven's	ORD	2022	N	Y	22.4	heavy	N	9.165	0.49	0.000416	Historic	-103.128	37.8679
Raven's	ORD	2022	N	Y	5.2	heavy	N	9.658	0.49	0.0279	Historic	-103.13	37.86735
Raven's	ORD	2022	Y	Y	40.3	heavy	Y	9.659	0.49	0.0301	Historic	-103.13	37.86736
Raven's	ORD	2021	Y	Y	33.9	heavy	Y	9.661	0.49	2.09E-05	Historic	-103.13	37.86748
Raven's	ORD	2021	Y	Y	27.4	heavy	N	9.667	0.49	1.13E-05	Historic	-103.13	37.86759
Raven's	ORD	2021	N	Y	14.3	heavy	N	9.672	0.43	1.73E-05	Historic	-103.131	37.86765
Raven's	ORD	2022	N	Y	5.3	heavy	N	9.827	0.43	0.00563	Historic	-103.133	37.86821
Raven's	ORD	2021	N	N	62.3	bare	Y	9.931	0.32	0.00884	Historic	-103.134	37.87049
Raven's	ORD	2021	N	N	54.7	bare	N	54.008	0.43	2.09E-05	Historic	-103.135	37.87164
Raven's	ORD	2021	Y	Y	46.1	heavy	N	54.020	0.43	0	Historic	-103.136	37.87197
Raven's	ORD	2022	N	Y	33.9	heavy	Y	55.406	0.32	1.69E-05	Historic	-103.137	37.87444
Raven's	ORD	2022	Y	Y	5.0	heavy	N	0.440	0.32	0.0226	Historic	-103.136	37.87514
Raven's	ORD	2022	Y	Y	8.3	heavy	N	0.428	0.32	0.0116	Historic	-103.135	37.87516
Raven's	ORD	2022	N	Y	19.8	heavy	N	0.010	0.49	0.0236	Historic	-103.133	37.87477
Raven's	ORD	2022	N	Y	9.5	heavy	N	0.364	0.49	0.0330	Historic	-103.134	37.87449
Raven's	ORD	2021	N	N	38.0	sparse	N	43.434	0.43	2.02E-05	Historic	-103.135	37.85986
Raven's	ORD	2021	Y	Y	38.9	heavy	N	43.436	0.43	1.82E-05	Historic	-103.135	37.86002
Raven's	ORD	2021	N	N	62.4	sparse	Y	43.437	0.43	2.46E-05	Historic	-103.135	37.86012
Raven's	ORD	2021	N	N	30.9	heavy	Y	43.442	0.43	1.86E-05	Historic	-103.135	37.86057
Raven's	ORD	2021	Y	Y	60.1	sparse	N	43.447	0.43	0.00326	Historic	-103.135	37.86088
Raven's	ORD	2021	N	N	53.2	heavy	N	43.507	0.49	1.44E-05	Historic	-103.135	37.86134
Raven's	ORD	2021	N	N	53.2	sparse	N	43.510	0.49	1.82E-05	Historic	-103.135	37.8615
Raven's	ORD	2021	Y	Y	56.5	sparse	N	43.515	0.43	2.12E-05	Historic	-103.135	37.86186
Raven's	ORD	2021	N	N	54.2	heavy	N	43.527	0.43	0.00406	Historic	-103.135	37.8626
Raven's	ORD	2021	Y	Y	43.2	heavy	N	43.536	0.43	2.27E-05	Historic	-103.135	37.86275
Raven's	ORD	2021	N	N	37.5	heavy	N	43.550	0.43	1.73E-05	Historic	-103.135	37.86295

Raven's	ORD	2021	N	N	42.0	heavy	N	43.572	0.43	2.44E-05	Historic	-103.135	37.86361
Raven's	ORD	2021	Y	Y	26.5	heavy	N	43.870	0.43	1.51E-05	Historic	-103.135	37.86381
Raven's	ORD	2021	N	N	52.0	heavy	Y	43.896	0.43	2.09E-05	Historic	-103.135	37.86448
Raven's	ORD	2021	N	N	72.5	sparse	N	43.906	0.43	2.02E-05	Historic	-103.134	37.86472
Raven's	ORD	2021	N	N	65.2	heavy	N	43.910	0.43	1.65E-05	Historic	-103.134	37.86483
Raven's	ORD	2021	N	N	37.5	heavy	N	43.917	0.43	1.47E-05	Historic	-103.134	37.86506
Raven's	ORD	2021	N	N	29.6	heavy	N	43.939	0.49	1.64E-05	Historic	-103.134	37.86601
Raven's	ORD	2022	Y	Y	7.4	heavy	N	0.213	0.49	0.0396	Historic	-103.138	37.86602
Raven's	Zuni	2022	N	Y	7.2	heavy	N	0.208	0.49	0.00771	Historic	-103.138	37.86608
Raven's	ORD	2022	N	Y	1.8	heavy	N	0.005	0.49	0.0222	Historic	-103.139	37.86612
Raven's	ORD	2017	N	N	85.9	bare	N	57.387	0.24	2.34E-05	Historic	-103.143	37.88402
Heartland	Logs	2021	N	Y	90.0	heavy	N	0.254	0.32	0.0308	Historic	-102.897	37.67911
Heartland	Logs	2021	N	Y	3.3	heavy	N	0.251	0.32	0.0009	Historic	-102.896	37.67875
Heartland	PALS	2021	N	Y	33.0	heavy	N	0.250	0.32	0.0348	Historic	-102.896	37.67859
Heartland	ORD	2021	N	Y	23.5	heavy	N	0.244	0.32	0.000321	Historic	-102.896	37.67844
Heartland	Logs	2021	N	Y	90.0	heavy	Y	0.229	0.32	0.0658	Historic	-102.896	37.6782
Heartland	Logs	2021	N	Y	10.8	heavy	Y	0.009	0.32	0.0561	Historic	-102.896	37.67811
Heartland	Logs	2021	N	Y	23.6	heavy	Y	0.092	0.32	0.102	Historic	-102.896	37.6776
Heartland	Logs	2021	N	Y	3.0	heavy	N	0.123	0.32	0.0137	Historic	-102.895	37.67783
Heartland	Zuni	2021	N	Y	24.6	heavy	Y	0.089	0.24	0.0971	Historic	-102.894	37.67772
Heartland	ORD	2022	N	Y	11.2	heavy	N	0.713	0.24	0.0214	Historic	-102.873	37.69979
Heartland	ORD	2022	N	Y	44.1	heavy	N	0.714	0.24	0.0294	Historic	-102.873	37.69989
Heartland	ORD	2022	N	Y	18.1	heavy	N	0.715	0.24	0.0139	Historic	-102.873	37.70002
Heartland	ORD	2022	N	Y	44.4	heavy	N	0.717	0.24	0.0299	Historic	-102.872	37.70035
Heartland	Zuni	2022	N	Y	21.0	heavy	N	0.032	0.24	0.0346	Historic	-102.873	37.70065
Heartland	ORD	2022	N	Y	5.7	heavy	N	0.031	0.24	0.0370	Historic	-102.873	37.70055
Heartland	ORD	2022	N	N	8.3	heavy	N	2.828	0.24	0.0232	Historic	-102.867	37.70128
Heartland	Logs	2022	N	Y	86.7	heavy	Y	2.829	0.24	0.0134	Historic	-102.867	37.7013
Heartland	PALS	2024	Y	Y	57.8	heavy	N	81.719	0.37	0.00608	Recent	-102.857	37.82268

Heartland	PALS	2024	N	N	52.6	heavy	N	81.718	0.37	0.00468	Recent	-102.857	37.82267
Heartland	PALS	2024	N	N	40.6	heavy	N	81.717	0.37	0.00930	Recent	-102.857	37.8227
Heartland	PALS	2024	Y	Y	33.4	heavy	N	81.713	0.37	0.0167	Recent	-102.858	37.82274
Heartland	PALS	2024	N	N	26.1	heavy	N	81.708	0.37	0.0170	Recent	-102.858	37.82278
Heartland	BDA	2024	Y	Y	9.4	heavy	N	82.605	0.49	2.29E-05	Recent	-102.857	37.82294
Heartland	BDA	2024	N	N	21.4	heavy	N	81.706	0.37	0.00584	Recent	-102.858	37.82289
Heartland	BDA	2024	Y	Y	10.2	heavy	N	81.706	0.37	0.00568	Recent	-102.858	37.82289
Raven's	ORD	2017	N	N	82.3	bare	Y	971.250	0.37	2.86E-05	Historic	-103.148	37.87991